Vol. 12, No. 2, June 30, 2021
Since 2010

ISSN 2233-4203 (print)
e-ISSN 2093-8950

Mass Spectrometry Letters

Screening of Nitrosamine Impurities in Sartan Pharmaceuticals by GC-MS/MS

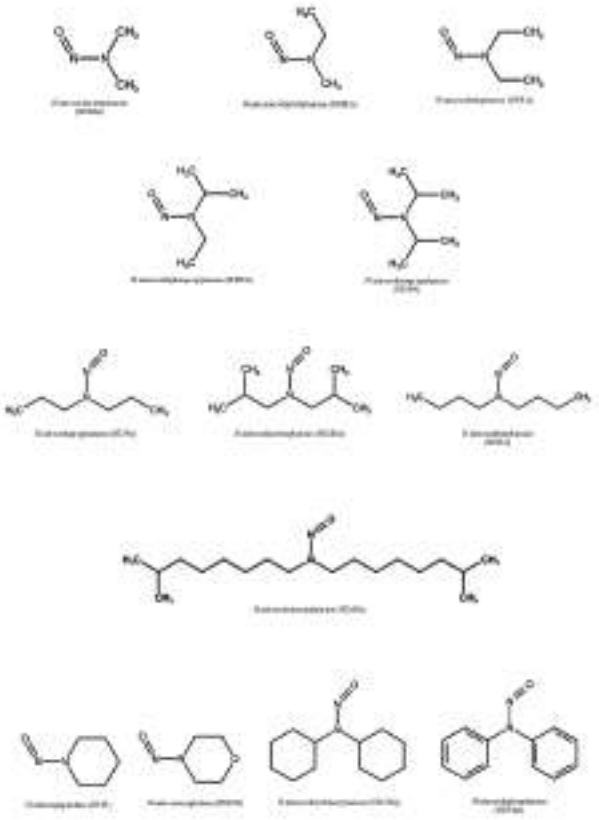

KSMS Korean Society for Mass Spectrometry

Mass Spectrometry Letters
Vol. 12, No. 2, June 30, 2021
The Korean Society for Mass Spectrometry

Mass Spectrometry Letters

ISO Abbreviation: *Mass Spectrom. Lett.*
Websites: www.msletters.org; msletters.koar.kr

Editorial Office
Administration office of the Korean Society for Mass Spectrometry
78 Daejeon Dunsan P.O.Box, 111 Dunsan-ro, Seo-gu, Daejeon, 35239, Republic of Korea
Contact: Yae Jin Joo
Homepage: www.ksms.org
E-mail: ksms@ksms.org
Tel: 82-70-8688-1696
Fax: 82-43-240-5159

MASS SPECTROMETRY LETTERS is indexed in Academic Society Village (http://society.kisti.re.kr), NDSL (National Discovery for Science Leaders, http://www.ndsl.kr), KSCI (Korea Science Citation Index, http://ksci.kisti.re.kr), KCI (Korea Citation Index, http://www.kci.go.kr), Chemical Abstracts (http://cas.org), and Scopus (www.scopus.com).

The journal hardcopy is distributed free to all the KSMS members who pay the membership fee in the corresponding year or at the cost of 20 US dollars/year to non-members.

Subscription information
Mass Spectrometry Letters follows ‘OPEN ACCESS’policy. One who wants to have an access to the full text is recommended to visit the Mass Spectrometry Letters official website (http://www.msletters.org/).
The printed material is sent to all the members of the KSMS for free and anyone who wants to receive the printed journal in Korea is strongly recommended to enroll in the KSMS. The membership fee information can be found in the KSMS homepage (www.ksms.org). One who wants to receive the printed journal abroad should contact Yae Jin Joo for more information.

Mass Spectrometry Letters Vol. 12, No. 2

Printed on June 25, 2021
Published on June 30, 2021

Publisher: Young Hwan Kim, President of KSMS
Publication Office: The Korean Society for Mass Spectrometry
Published since December 2010
Frequency of publication: 4 issues/year
The number of circulation of the printed journal: 400 copies/issue
Printed by Hanrimwon, Seoul, Korea, Tel: 82-2-2273-4201
ISSN 2233-4203 (print)
e-ISSN 2093-8950

Aims and Scope

Mass Spectrometry Letters publishes brief letters (maximum length of 4 pages), technical notes, articles, reviews, and tutorials on fundamental research and applications in all areas of mass spectrometry. The manuscripts can be either invited by the editors or submitted directly by authors to the journal editors. Mass Spectrometry Letters topical sections are diverse, covering ion chemistry in a broad sense; gas-phase thermodynamics or kinetics; theory and calculations related with mass spectrometry or ions in vacuum; ion-optics; analytical aspects of mass spectrometry; instrumentations; methodology developments; ionization methods; proteomics and its related research; metabolomics and its related research; bioinformatics; software developments; database development; biological research using mass spectrometry; pharmaceutical research by mass spectrometry; food sciences using mass spectrometry; forensic results using mass spectrometry; environmental mass spectrometry; inorganic mass spectrometry; chromatography-mass spectrometry; tandem mass spectrometry; small molecule research using mass spectrometry; TOF-SIMS, etc. The scope of Mass Spectrometry Letters is not limited to the above-mentioned areas, but includes ever-expanding areas related directly or indirectly to mass spectrometry. Criteria for publication are originality, urgency, and reportable values. Short preliminary or proof-of-concept results, which will be further detailed by the following submission to other journals, are recommended for submission.

CONTENTS

Volume 12, Number 2
June 2021

ARTICLE

Vol. 12, No. 2, 2021
ISSN 2233-4203/ e-ISSN 2093-8950
ARTICLE
www.msletters.org | Mass Spectrometry Letters

Screening of Nitrosamine Impurities in Sartan Pharmaceuticals by GC-MS/MS

Shu-Han Chang, Hui-Yu Ho, Chi-Zong Zang*, Ya-Hui Hsu, Mei-Chih Lin, Su-Hsiang Tseng, and Der-Yuan Wang

Food and Drug Administration, Ministry of Health and Welfare, Taipei, Taiwan

Received in April 22, 2021; Revised May 11, 2021; Accepted May 18, 2021
First published on the web June 30, 2021; DOI: 10.5478/MSL.2021.12.2.31

Abstract : Probable human carcinogenic compounds nitrosamines, have been detected as by-product impurities in sartan pharmaceuticals in recent years which has drawn worries for medication safety. To provide a sensitive and effective method for the quality control of sartan pharmaceuticals, this study established a feasible gas chromatography–tandem mass spectrometry (GC–MS/MS) method for simultaneous determination of 13 nitrosamines. The target analytes were separated on a DB-WAX Ultra Inert column (30 m × 0.25 mm; i.d., 0.25 μm) and were then subjected to electron impact ionization in multiple reaction monitoring mode. The established method was validated and further employed to analyze authentic samples. Limits of detection (LODs) and limits of quantification (LOQs) of the 13 nitrosamines were 15-250 ng/g and 50-250 ng/g, respectively, which also exhibited intra-day and inter-day accuracies of 91.4-104.8%, thereby satisfying validation criteria. Five nitrosamines, viz., *N*-nitrosodiethylamine, *N*-nitrosodimethylamine, *N*-nitrosodiphenylamine, *N*-nitrosomorpholine, and *N*-nitrosopiperidine were detected at concentrations above their LODs in 68 positive samples out of 594 authentic samples from seven sartans.

Keywords : angiotensin II type 1 receptor blockers, carcinogens, gas chromatography, mass spectrometry, nitrosamines

Introduction

Nitrosamines, analog compounds that include the same *N*-nitroso core structure (–N–N=O), are considered probable human carcinogens; these compounds are generally found in industrial manufacturing processes and environments.[1] In common industries, such as the food, cigarette, cosmetics, dye, pesticide, polymer, rubber, steel, and pharmaceutical sectors, nitrosamines are present as by-product impurities in the final products or as waste released into the environment.[2] The formation of a nitrosamine involves a series of complex reactions. While the mechanism of formation remains unclear, it is understood to involve nitrosation by nitrite, which, in turn, is affected by various factors, including the employments of amines, nitrates, and nitrites, as well variations of reaction conditions (such as pH, content, and concentration of the precursors).[3,4] The oxidation of unsymmetrical dimethylhydrazine (UDMH) and the chlorination of nitrites can also lead to the formation of nitrosamines.[5]

The evaluated excess lifetime cancer risk posed by nitrosamines is 10^{-5}–10^{-6} in the 0.7–100 ng/L concentration range for drinking water.[6,7] Since nitrosamines probably pose cancer risks to humans, several have been regulated by the international organizations or countries. For example, *N*-nitrosodiethylamine (NDEA) and *N*-nitrosodimethylamine (NDMA) have been categorized as Group 2A substances (probably carcinogenic to humans) by the World Health Organization (WHO), Group 1B substances (presumed to have carcinogenic potential for humans) in the European Union, and Group 2B substances (probable human carcinogens) in the USA. In addition, *N*-nitrosodipropylamine (NDPA), *N*-nitrosomethylethylamine (NMEA), *N*-nitrosomorpholine (NMOR), and *N*-nitrosopiperidine (NPIP) are categorized as Group 2B substances (possibly carcinogenic to humans) by the WHO.[7,8]

NDMA, an impurity present in valsartan, was detected and reported by Spain in 2018, which was announced via the PIC/S Rapid Alert System. Initially, this unexpected impurity was ascribed to a change in the manufacturing process of valsartan active pharmaceutical ingredient (API) by a Chinese pharmaceutical company.[9,10] Subsequently, more countries have reported the cases of nitrosamine-contaminated sartan medicines.[11-13] From these reports, the nitrosamine contamination of sartan medicines has become an urgent issue in the world-wide quality control of pharmaceuticals.

Sartans are classified as angiotensin II receptor type 1 antagonists and are widely used to treat cardiovascular

*Reprint requests to Chi-Zong Zang, orcid.org
https://orcid.org/0000-0002-5633-876X
E-mail: heavenincry@fda.gov.tw

diseases, such as hypertension, heart failure, and myocardial infarction.[14,15] While minor impurities, such as the degraded fragments of the target compounds, are produced within the synthesis of sartan APIs, nitrosamines are not generally expected to be produced following the methods applied for synthesizing sartan API.[16-18] Unfortunately, some alterations to the synthetic protocols have led to the formation of nitrosamines. For example, the solvent used in the recovery process can lead to the formation of nitrosamines. The aprotic polar solvent used to manufacture sartans, especially dimethylformamide (DMF), is recycled and quenched with sodium nitrite ($NaNO_2$) to remove residual azide formed through the use of anhydrous zinc chloride ($ZnCl_2$) and sodium azide (NaN_3), which leads to the formation of NDMA.[19,20]

Since nitrosamines are probably carcinogenic to humans, establishing an analytical method for the detection of nitrosamines in pharmaceutical products has become an important objective. Literatures have reported methods for determining nitrosamines based on liquid chromatography coupled with tandem mass spectrometry (LC–MS/MS).[21,22] On contrast, several research teams have developed analytical methods for few nitrosamines based on gas chromatography–mass spectrometry GC–MS and GC–MS/MS methods.[23,24] This study aimed to develop a GC–MS/MS method of larger coverage for the screening of 13 nitrosamines in sartan medicines. The established method was validated and further employed to analyze authentic sartan medicines.

Materials and Methods

Chemicals and reagents

N-Nitrosodibutylamine (NDBA), NDEA, NDMA, NDPA, NDMA-d_6, and NDPA-d_{14} were purchased from AccuStandard (CT, USA). *N*-Nitrosoethylisopropylamine (NEIPA), *N*-nitrosodiisopropylamine (NDiPA), and NMOR were purchased from BOC Sciences (NY, USA), Chem Service (PA, USA), and Sigma-Aldrich (MO, USA), respectively. *N*-Nitrosodiphenylamine (NDPhA) and NPIP were purchased from Supelco (PA, USA). *N*-Nitrosodiisobutylamine (NDiBA), *N*-nitrosodicyclohexylamine (NDCHA), *N*-nitrosodiisononylamine (NDiNA), NMEA, *N*-nitrosodiethylamine-d_4 (NDEA-d_4), and *N*-nitrosodiphenylamine-d_{10} (NDPhA-d_{10}) were acquired from TRC (ON, Canada). Chromatography-grade methanol was obtained from Sigma-Aldrich (MO, USA). The chemical structures of the 13 nitrosamines analyzed in this study are shown in Fig. 1. A total of 594 authentic samples of seven sartans, viz. azilsartan medoxomil (19 final products), candesartan cilexetil (4 APIs and 6 final products), irbesartan (35 APIs and 28 final products), losartan (68 APIs and 198 final products), olmesartan medoxomil (8 APIs and 18 final products), telmisartan (18 final products), and valsartan (65 APIs and 127 final products), were collected by local public health bureaus in Taiwan and analyzed in this study.

Instrumentation and chromatographic conditions

The experiments were conducted on a GC–MS/MS system in which a 7890B GC instrument was coupled to a 7000C triple quadrupole mass spectrometer, both from Agilent Technologies (Santa Clara, CA, USA). Data acquisition and processing were performed using Agilent Mass Hunter Quantitative Analysis B.06.00 and Mass Hunter Qualitative software. Chromatography was performed using an Agilent Technologies DB-WAX Ultra Inert column (30 m × 0.25 mm; i.d., 0.25 μm), with the performance of an Agilent J&W HP-5MS column (30 m × 0.25 mm; i.d., 0.25 μm) and an Agilent DB-624 column (60 m × 0.25 mm; i.d., 1.40 μm) was also examined. The carrier gas (helium) was set to a constant flow rate of 1 mL/min. The GC operating parameters were as follows: pulsed splitless injection mode, inlet temperature 250°C, and interface temperature 250°C. The GC temperature program was set as follows: the initial temperature of 80°C was held for 3.0 min, after which it was raised to 250°C at 20°C/min and held for 3 min. A sample injection volume of 2 μL was applied. The total chromatographic run time was 14.5 min. The mass spectrometer was operated in electron impact (EI) ionization mode under the following conditions: ionization energy 70 eV, ion source temperature 230°C, and 1st & 2nd quadrupole temperature 150°C. Analytes were monitored in multiple reaction monitoring (MRM) mode. The MRM parameters, including the MRM transitions, quantifiers, qualifiers, and collision energies, are provided in Table 1.

Standard solution preparation

Stock solutions of the 13 nitrosamines and four internal standards (ISs) were prepared in methanol at concentrations of 1000 μg/mL. The IS stock solution was diluted with methanol to prepare 200 ng/mL IS solutions. Calibration curves for the nitrosamines were prepared at seven points in the 1–50 ng/mL concentration range, including the IS of equivalent 20 ng/mL. All the stock and working solutions were stored at -30°C. All reagents were brought to controlled room temperature prior to use.

Sample preparation

Sartan matrices (100 mg; API or ground tablet powder), IS solutions (500 μL; 200 ng/mL), and 4.5 mL of methanol were transferred to a 15-mL centrifuge tube and mixed well to form a homogeneous solution. It should be noted that methanol was replaced with the standard solution of interest for validation purposes. Each solution was sonicated for 30 min and then filtered through a 0.22-μm polyvinylidene fluoride (PVDF) filter. The filtrate was collected as the sample solution and subjected to analysis in this study.

Method validation

Linearity and sensitivity

Linearity was assessed by least-squares linear regression analysis of the calibration curves. The calibration curves were constructed by plotting the peak area ratio of the

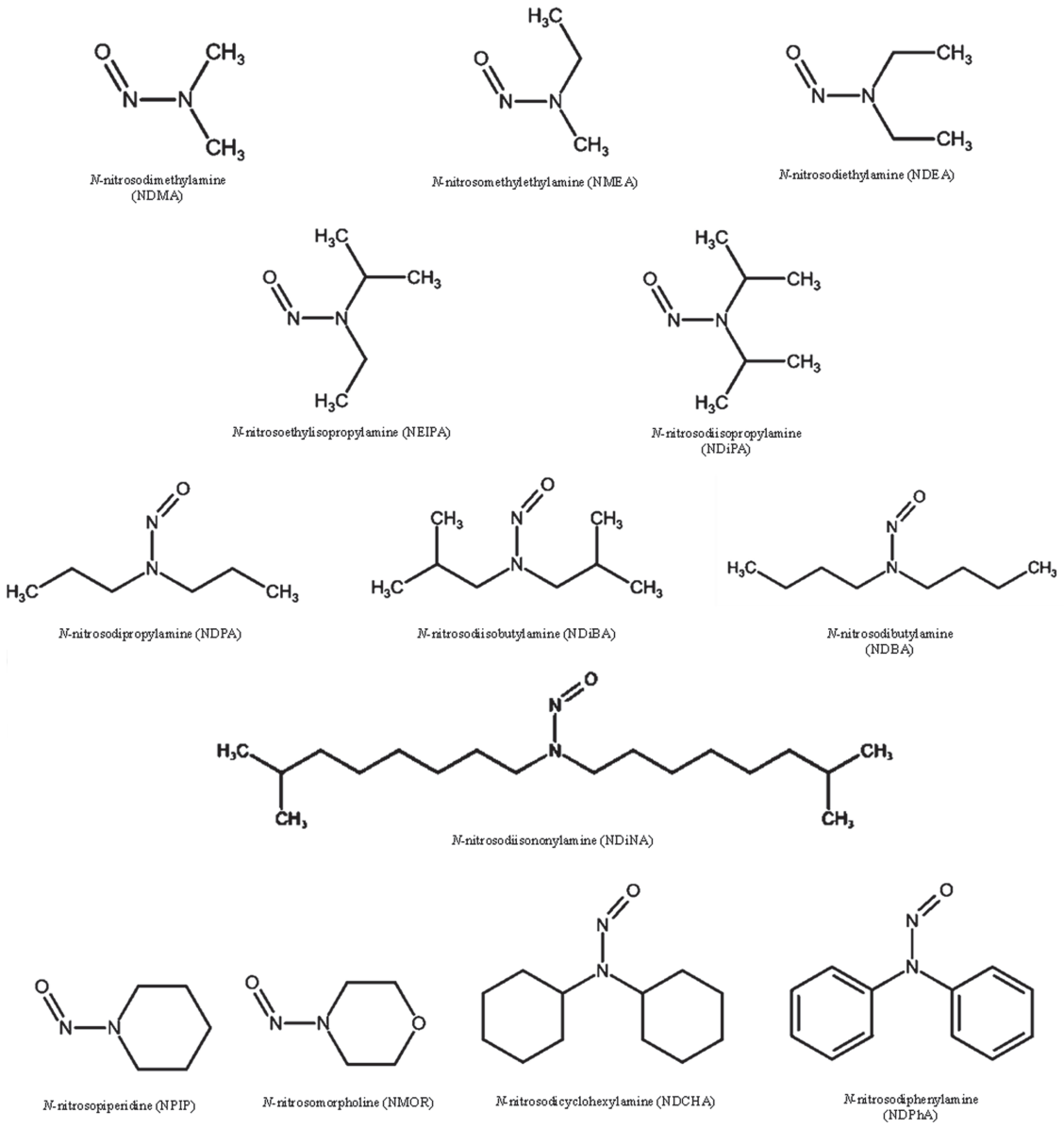

Figure 1. Chemical structures of the 13 nitrosamines.

standard solution vs. IS determined by the analysis of 13 standard solutions with concentration range of 1–50 ng/mL. The acceptable value for the correlation coefficient (r) was 0.995 and above. The limits of detection (LOD) and quantification (LOQ) were selected as indices of sensitivity and evaluated following the validation protocol of the International Council for Harmonisation (ICH).[25] The LOD and LOQ were determined based on signal-to-noise (S/N) ratios of 3 and 10, respectively, whereas ± 20% was set as the ion-ratio criterion.

Accuracy and precision

Prior to any assessment, the sartan matrices were examined to ensure that no nitrosamines were present as interferents. Accuracy, expressed as recovery (%), was determined through quality control (QC) based on intra-day and inter-day target analyte testing following the ICH procedure.[25,26] The QC criteria are referenced to those of the Taiwan Food and Drug Administration (TFDA): for 1-10 ng/mL, recoveries of 60-125% and an RSD < 30%; for 10-100 ng/mL, recoveries 70-120% and an RSD of 20%. Accuracy (%) was assessed by comparing the concentration of the analyte determined in the matrix (A) with the concentration of the standard solution (B) as follows: [A]/[B] × 100%. Precision (RSD in %) was assessed at three concentrations (5, 25, and 50 ng/mL) on the same day (n = 3) and over three consecutive days (n = 9).

Table 1. MRM parameters for the 13 nitrosamines and four ISs.

Analyte	Retention time (min)	MRM transition (*m/z*)	Dwell time (ms)	CE (eV)
NDMA	5.004	74 > 42 [a] 74 > 44	80	20 13
NMEA	5.556	88 > 71 [a] 88 > 42	45	2 15
NDEA	5.875	102 > 85 [a] 102 > 56	45	2 15
NEIPA	6.225	116 > 99 [a] 116 > 44	55	2 12
NDiPA	6.470	130 > 88 [a] 130 > 42	55	2 10
NDPA	7.113	130 > 113 [a] 130 > 43	40	2 13
NDiBA	7.278	115 > 84 [a] 103 > 57	40	2 8
NDBA	8.412	116 > 99 [a] 158 > 99	100	2 5
NPIP	8.643	114 > 84 [a] 114 > 97	55	10 5
NMOR	9.139	116 > 86 [a] 116 > 56	55	2 13
NDiNA	11.606	169 > 99 [a] 281 > 225	100	12 12
NDCHA	12.638	210 > 128 [a] 210 > 111	150	5 2
NDPhA	13.141	169 > 168 [a] 169 > 167	65	18 30
NDMA-d_6	4.996	80 > 46 [a]	80	18
NDEA-d_4	5.873	106 > 88 [a]	45	2
NDPA-d_{14}	7.049	110 > 78 [a]	40	2
NDPhA-d_{10}	13.123	179 > 177 [a]	80	18

[a] quantifier; CE: collision energy; MRM: multiple reaction monitoring

Results and Discussion

GC–MS/MS method development

As part of the optimization process, the efficacy of different columns was investigated in order to determine which was the most suitable for the chromatographic analysis of the target analytes. Several columns have reportedly been used to detect nitrosamines in non-water matrices. Santillana et al. reported a GC–MS method for the detection of eight nitrosamines in polymer teats and soothers by applying an Agilent DB-624 column in which the overall run time of the method was 30 min.[27] The U.S. FDA has specified GC–MS and GC–MS/MS methods for the detection of nitrosamines in valsartan that use Agilent DB-WAX and VF-WAXms columns with overall run times for both methods of less than 20 min.[28,29] In the current study, the three columns described in the "Instrumentation and chromatographic conditions" section were examined. The 13 nitrosamines (50 μg/mL in methanol) were separately analyzed in full scan mode using the three columns and the temperature program reported in the literature for the chromatographic separation of the target analytes.[29] Nevertheless, the reference method was not entirely suitable for this study because a larger number of nitrosamines was investigated; several analytes did not appear in the chromatogram within the run time, and the entire analysis process was inefficient, with loosely dispersed chromatographic peaks. Hence, the method was adjusted to improve the peak profile, with most analytes finally separated by applying the temperature program described in "Instrumentation and chromatographic conditions" section. However, discrepancies of the individual columns were observed in the chromatographic separations, which are ascribable to the polarity difference among the target analytes and columns. NDMA and NMEA were coincident with the solvent peak (3 min) using the HP-5MS column, owing to the high polarity of both analytes, while the remaining 11 nitrosamines exhibited split peaks. On the other hand, NDiNA, NDCHA, NDELA, and NDiPLA were not detected using the DB-624 column, whereas the peaks for the remaining nine nitrosamines were asymmetric. In contrast, the DB-WAX Ultra Inert column demonstrated good resolution (more than 0.1 min between adjacent analytes) and symmetric peaks for all 13 nitrosamines. Based on these results, DB-WAX Ultra Inert column was adopted for further method development.

The MS/MS conditions were optimized in order to select the best precursor and product ions for each analyte based on the ions collected in full scan mode (in the 50–300 *m/z* range). The ionization energy was appropriately set in order to optimally fragment each analyte since the ionization energy would affect screening efficacy and target analyte quantification. The lower ionization energy 40 eV has been reportedly used to determine multiple nitrosamines.[29] Therefore, the ionization energy was initially set at 40 eV in this study. However, the scale of this energy level was found to be insufficient to fragment those nitrosamines with larger molecular weights. Consequently, the ionization energy was adjusted to the higher level 70 eV; at this energy level, all 13 nitrosamines were successfully ionized to generate fragments suitable for MRM mode. The MRM parameters for the 13 nitrosamines and 4 ISs are listed in Table 1, whereas the total ion chromatograms (TICs) of GC analysis and MRM chromatograms for mass fragment are displayed in Figure 2 and Figure 3, respectively. Although the qualifiers and quantifiers of the analytes were determined according to the relative intensities of the precursor and product fragments, specific scenarios needed to be considered. For example, the matrix can contribute ions to the analytes in MRM mode. In this study, the matrix interfered with the 210 > 193 *m/z* qualifier ions

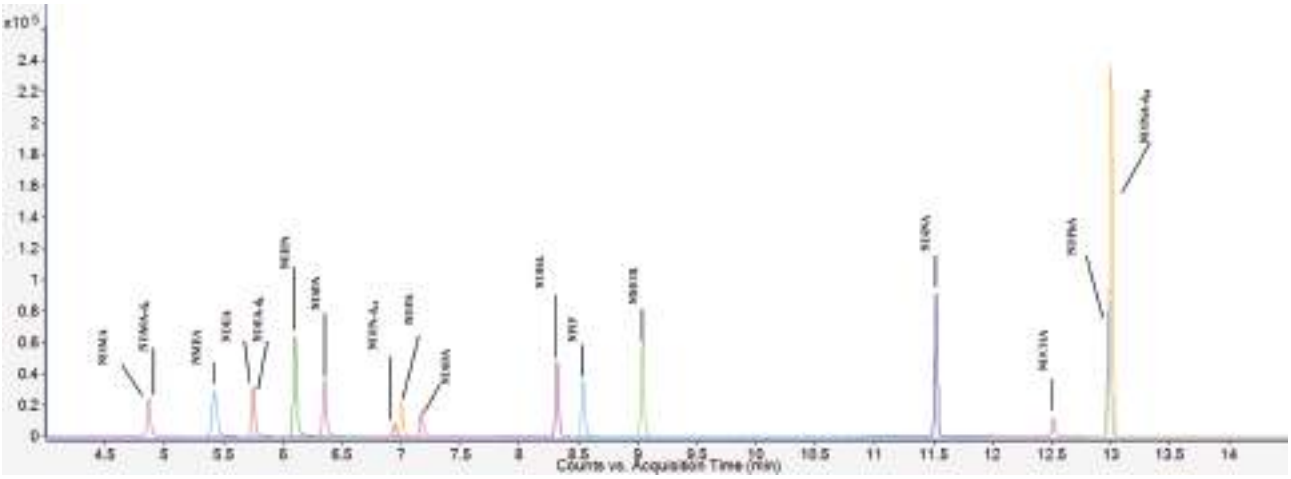

Figure 2. Total ion chromatogram of the 13 nitrosamines (25 ng/mL) and four ISs (20 ng/mL).

for NDCHA; hence, to avoid incorrect assignments, the 210 > 111 (*m/z*) qualifier ions were used instead, which helped to diminished interference from the matrix.

Method validation

Linearity and sensitivity

The calibration curves for the 13 nitrosamines were assessed in the 1-50 ng/mL concentration range, with the criterion of correlation coefficient (*r*) for each analyte set to 0.995 and above. The *r* values for all 13 nitrosamines exceeded 0.995 (data shown in Table S1 of supplemental data), revealing sufficient linearity in the concentration range and indicating that the ISs used are suitable for the quantification of the target analytes by applying the developed method. The LOD and LOQ for each nitrosamine in each sartan matrix, including the APIs and final products, were determined and the data are listed in Table 2. The lower limits were achieved for most analytes during qualification and quantification; however, the matrices significantly hindered quantification ions of analytes at low concentrations, which affected the determination of LOD and LOQ. This hindering effect is attributable to the components of the matrices of final products, such as the excipients, whereas few hindering effects were observed for the API matrices. Among all matrices, that of the losartan final product hindered most analytes, including NDMA, NMEA, NDPA, NDiBA, NMOR, and NDCHA. To diminish the hindering effects of the matrices on LOD determination, solid phase extraction (SPE) was applied to purify the samples. Several cartridges (Agilent Bond Elut C18, 50 mg, 40 µm, 3 mL; Oasis MCX Vac, 60 mg, 30 µm, 3 mL; Oasis HLB Vac, 60 mg, 30 µm, 3 mL) and elution conditions were examined; however, no remarkable improvement was observed owing to poor recoveries, which made improving the LODs of the analytes difficult.

GC–MS and GC–MS/MS methods have been developed for determining nitrosamines in sartans. The U.S. FDA established a GC–MS/MS method for determining five nitrosamines for which LODs of 1–10 ng/g were observed for sartan APIs and 2–16 ng/g for sartan final products. Furthermore, LOQs were observed to range from 5 to 25 ng/g in sartan APIs and from 8 to 40 ng/g in sartan final products.[29] Health Canada announced a GC–MS/MS method for detecting NDMA and NDEA in sartan APIs, with LODs of 2 ng/g for both nitrosamines, and LOQs of 5.4 ng/g and 7.3 ng/g, respectively.[30] Compared to the methods reported in the literature, the GC–MS/MS method developed in this study is effective for a larger variety of analytes and displays sufficient sensitivity for the detection and determination of nitrosamines in sartans.

Accuracy and precision

The intra-day accuracies for the 13 analytes in the sartan APIs were determined to be 97.0-103.5% with precisions of 0.5-9.7%, whereas these values were 91.4-104.2% and 1.2-7.9% for the sartan final products, respectively. The 13 analytes in the sartan APIs exhibited inter-day accuracies of 97.8-104.8% with precisions of 1.5-12.2%, whereas the sartan final products exhibited values of 92.9-103.3% and 1.6-7.1%, respectively. Therefore, the accuracies and precisions of the 13 analytes in the sartan matrices, including the APIs and the final products, are compliant with the criteria set in "Accuracy and precision" section (all data were shown in Table S2 and S3 of supplemental data).

Application to authentic samples

The validated method was further applied to analyze the sartan samples collected from the pharmacies and pharmaceutical manufacturers. A total of 594 authentic samples from seven sartans were analyzed, the results of which are summarized in Table 3. Five nitrosamines,

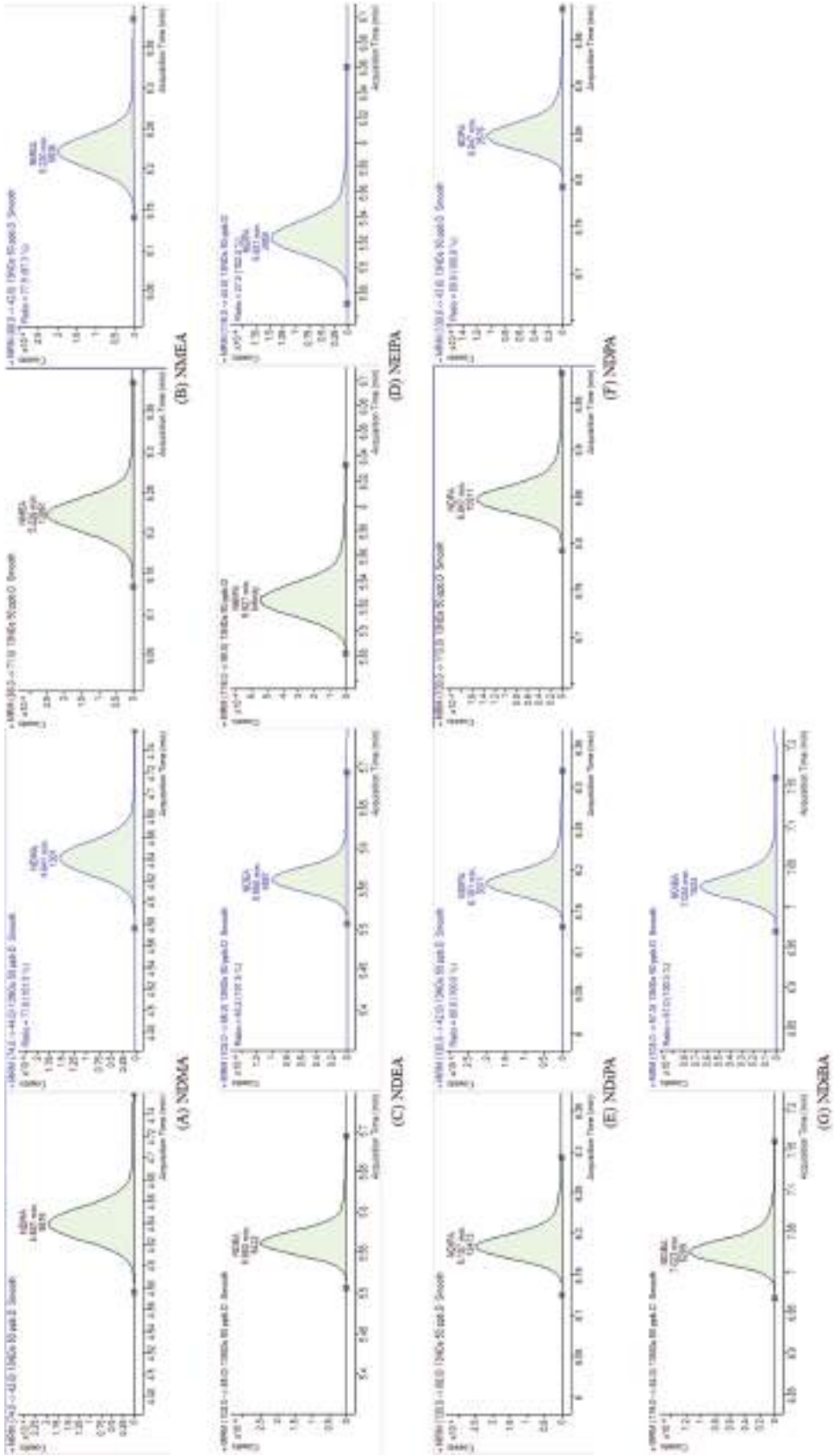

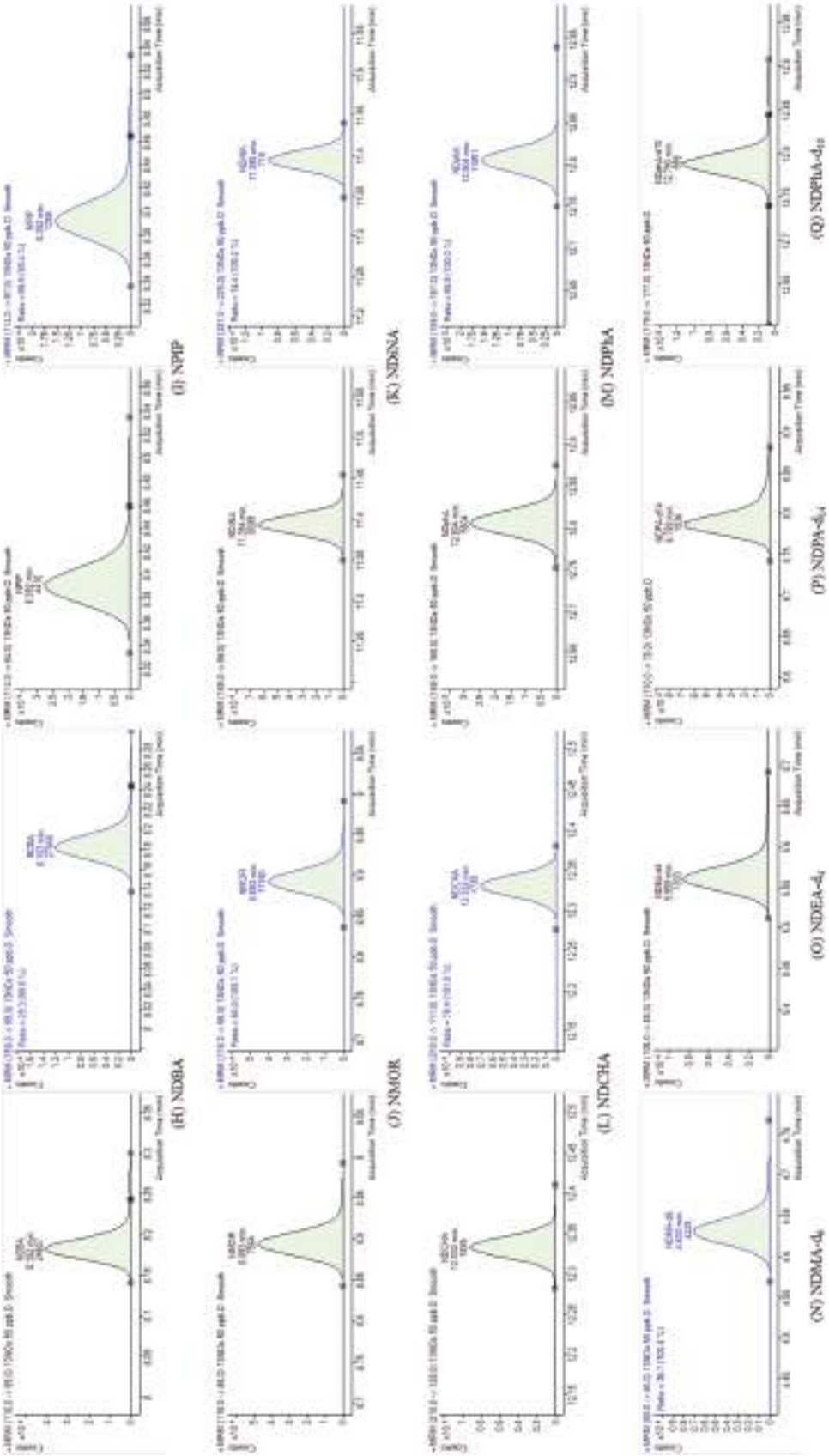

Figure 3. Chromatograms of transition ions for 13 nitrosamines (qualifier in left and quantifier in right) and four ISs (quantifier only) under MRM mode.

Table 2. LODs and LOQs for the 13 nitrosamines (APIs).

Analyte	Matrix									
	Candesartan cilexetil		Irbesartan		Losartan		Olmesartan medoxomil		Valsartan	
	LOD (μg/g)	LOQ (μg/g)	LOD (μg/g)	LOQ (μg/g)	LOD (μg/g)	LOQ (μg/g)	LOD (μg/g)	LOQ (μg/g)	LOD (μg/g)	LOQ (μg/g)
NDMA	0.025	0.05	0.025	0.05	0.025	0.05	0.25	0.25	0.025	0.05
NMEA	0.025	0.05	0.025	0.05	0.025	0.05	0.025	0.05	0.015	0.05
NDEA	0.025	0.05	0.025	0.05	0.025	0.05	0.015	0.05	0.025	0.05
NEIPA	0.025	0.10	0.025	0.10	0.015	0.10	0.015	0.10	0.025	0.15
NDiPA	0.015	0.05	0.015	0.05	0.015	0.05	0.025	0.05	0.015	0.05
NDPA	0.25	0.25	0.025	0.05	0.025	0.05	0.025	0.05	0.015	0.05
NDiBA	0.05	0.10	0.05	0.10	0.05	0.10	0.10	0.10	0.05	0.10
NDBA	0.015	0.05	0.015	0.05	0.015	0.05	0.015	0.05	0.025	0.05
NPIP	0.015	0.05	0.025	0.05	0.015	0.05	0.025	0.05	0.025	0.05
NMOR	0.025	0.05	0.025	0.05	0.015	0.05	0.025	0.05	0.025	0.05
NDiNA	0.025	0.05	0.025	0.05	0.025	0.05	0.025	0.05	0.025	0.05
NDCHA	0.025	0.05	0.025	0.05	0.025	0.05	0.025	0.05	0.025	0.05
NDPhA	0.015	0.05	0.015	0.05	0.015	0.05	0.05	0.05	0.015	0.05

Note: Five sartan APIs merchandised in Taiwan were tested.

Table 2. (Continued, final products)

Analyte	Matrix													
	Azilsartan medoxomil		Candesartan cilexetil		Irbesartan		Losartan		Olmesartan medoxomil		Telmisartan		Valsartan	
	LOD (μg/g)	LOQ (μg/g)	LOD (μg/g)	LOQ (μg/g)	LOD (μg/g)	LOQ (μg/g)	LOD (μg/g)	LOQ (μg/g)	LOD (μg/g)	LOQ (μg/g)	LOD (μg/g)	LOQ (μg/g)	LOD (μg/g)	LOQ (μg/g)
NDMA	0.30	0.30	0.025	0.05	0.05	0.05	0.25	0.25	0.25	0.25	0.10	0.15	0.025	0.05
NMEA	0.025	0.05	0.015	0.05	0.025	0.05	0.025	0.05	0.10	0.10	0.025	0.05	0.025	0.05
NDEA	0.05	0.05	0.025	0.05	0.025	0.05	0.025	0.05	0.015	0.05	0.025	0.05	0.025	0.05
NEIPA	0.05	0.10	0.05	0.10	0.025	0.10	0.05	0.10	0.05	0.15	0.05	0.10	0.05	0.10
NDiPA	0.025	0.05	0.015	0.05	0.025	0.05	0.025	0.05	0.025	0.05	0.05	0.05	0.025	0.05
NDPA	0.025	0.05	0.05	0.05	0.025	0.05	0.15	0.15	0.15	0.15	0.05	0.10	0.015	0.05
NDiBA	0.25	0.25	0.05	0.05	0.05	0.05	0.05	0.05	0.05	0.05	0.10	0.15	0.05	0.05
NDBA	0.025	0.05	0.015	0.05	0.015	0.05	0.015	0.05	0.015	0.05	0.025	0.05	0.025	0.05
NPIP	0.025	0.05	0.015	0.05	0.015	0.05	0.015	0.05	0.025	0.05	0.025	0.05	0.025	0.05
NMOR	0.025	0.05	0.05	0.05	0.015	0.05	0.05	0.05	0.025	0.05	0.05	0.05	0.025	0.05
NDiNA	0.015	0.05	0.015	0.05	0.015	0.05	0.015	0.05	0.025	0.05	0.05	0.10	0.025	0.05
NDCHA	0.025	0.05	0.025	0.05	0.025	0.05	0.25	0.25	0.25	0.25	0.025	0.15	0.05	0.05
NDPhA	0.015	0.05	0.025	0.05	0.015	0.05	0.015	0.05	0.015	0.05	0.025	0.05	0.025	0.05

including NDMA, NDEA, NDPhA, NMOR, and NDIP were detected at concentrations above their LODs in 68 positive samples of losartan, irbesartan, and valsartan. Among the samples, the valsartan products included 57 positive samples (duplicated samples excluded) with the highest nitrosamine contents (NDMA, 99,790 ng/g). In addition, these positive samples were found to contain multiple targets, with NDEA detected most frequently in these samples. On the basis of these results, we conclude that the developed method is a sensitive and effective technique for monitoring and quantifying multiple nitrosamines in sartans.

Table 3. Nitrosamines detected in authentic sartan samples.

Target	Item	Sartan		
		Valsartan (192 pcs)	Losartan (266 pcs)	Irbesartan (63 pcs)
NDMA	Positive samples (pcs)	54	0	0
	Detection rate (%)	28.1	-	-
	Content (μg/g)	0.06-99.79	ND	ND
NDEA	Positive samples (pcs)	11	4	5
	Detection rate (%)	5.7	1.5	7.9
	Content (μg/g)	0.11-8.84	0.07-0.20	0.10-0.14
NDPhA	Positive samples (pcs)	1	1	1
	Detection rate (%)	0.5	0.4	1.6
	Content (μg/g)	0.12	0.10	0.06
NMOR	Positive samples (pcs)	2	0	0
	Detection rate (%)	1.0	-	-
	Content (μg/g)	0.16	ND	ND
NPIP	Positive samples (pcs)	2	0	0
	Detection rate (%)	1.0	-	-
	Content (μg/g)	0.12	ND	ND

Conclusion

In this study, we successfully developed a GC–MS/MS method for monitoring and determining 13 nitrosamines in sartans. The method was validated and satisfactorily applied to analyze authentic samples. Therefore, the developed method can be used for quality-monitoring purposes during the manufacture of sartan pharmaceuticals.

Acknowledgments

This work was supported by the Food and Drug Administration, Ministry of Health and Welfare in Taiwan, R.O.C.

Supplementary Information

Supplementary Information is available at https://drive.google.com/file/d/1Q4BG0FwkaUrgXcqG3afYbOlYXqeIrqOM/view?usp=sharing.

References

1. Krauss, M.; Longrée, P.; van Houtte, E.; Cauwenberghs, J.; Hollender, J. *Environ. Sci. Technol.*, **2010,** 44, 7871, DOI: 10.1021/es101289z.
2. Mitch, W. A.; Sharp, J. O. R.; Trussell, R.; Valentine R. L.; Alvarez-Cohen, L.; Sedlak, D. L. *Environ. Eng. Sci*. **2003**, 20, 389, DOI: 10.1089/109287503768335896.
3. Chen, X.; Huang, G.; An, C.; Yao, Y.; Zhao, S. *Chem. Eng. J*. **2018**, 335, 921, DOI: 10.1016/j.cej.2017.11.032.
4. Piazzoli, A.; Breider, F.; Aquillon, C. G.; Antonelli, M.; von Gunten, U. *Water Res*. **2018**, 135, 311, DOI: 10.1016/j.watres.2018.02.019.
5. Kristiana, I.; Tan, J.; Joll, C. A.; Heitz, A; von Gunten, U.; Charrois, J. W. A. *Water Res*. **2013**, 47, 535, DOI: 10.1016/j.watres.2012.10.014.
6. Wang, W.; Hu, J.; Yu, J.; Yang, M. *J. Environ. Sci*. **2010**, 22, 1508, DOI: 10.1016/S1001-0742(09)60281-3.
7. Selin N. E. *Environmental Guidelines and Regulations for Nitrosamines: A Policy Summary, Final report revision 2. Engineering Systems and Atmospheric Chemistry Engineering Systems Division and Department of Earth, Atmospheric and Planetary Sciences*, Massachusetts Institute of Technology; Cambridge, MA.
8. European Medicines Agency. EMA reviewing medicines containing valsartan from Zhejiang Huahai following detection of an impurity (EMA/459276/2018). European Medicines Agency: London, **2018**. Accessed December 1, 2020.
9. White, C. M. *Ann. Pharmacother.* **2020**, 54, 611e4, DOI: 10.1177/1060028019892222.
10. European Medicines Agency, *Sartan Medicines: Companies to Review Manufacturing Processes to Avoid Presence of Nitrosamine Impurities*, **2019**. Available at: https://www.ema.europa.eu/en/news/sartan-medicines-companies-review-manufacturing-processes-avoid-presence-nitrosamine-impurities. Accessed July 14, 2020.
11. United States Food and Drug Administration, *List of Valsartan Products Under Recall*, **2018**. Available at: https://www.fda.gov/downloads/Drugs/DrugSafety/UCM615703.pdf. Accessed October 20, 2018. Accessed

December 1, 2020.
12. United States Food and Drug Administration, *FDA Updates and Press Announcements on Angiotensin II Receptor Blocker (ARB) Recalls (Valsartan, Losartan, and Irbesartan)*, Available at: https://www.fda.gov/drugs/drug-safety-and-availability/fda-updates-and-press-announcements-angiotensin-ii-receptor-blocker-arb-recalls-valsartan-losartan. Accessed November 07, 2019
13. Lim, H. H.; Oh, Y. S.; Shin, H. S. *J. Pharm. Biomed. Anal*. **2020**, 189, 113460. DOI: 10.1016/j.jpba.2020.113460.
14. Siddiqui, N.; Husain, A.; Chaudhry, L.; Alam, M. S.; Mitra, M.; Bhasin, P. S. *J. Appl. Pharm. Sci*. **2011**, 1, 12.
15. Muszalska, I.; Sobczak, A.; Dolhan, A.; Jelinska, A. *J. Pharm. Sci.* **2014**, 103, 2, DOI: 10.1002/jps.23760.
16. Srinivasan, V.; Sivaramakrishnan, H.; Karthikeyan, B. *Arab. J. Chem*. **2016**, 9, S1516, DOI: 10.1016/j.arabjc.2012.03.022.
17. Pandey, K. A.; Rapolu, R; Raju, C. K.; Sasalamari, G; Goud, K. S.; Awasthi, A; Navalgund, S. G.; Surendranath, K. V. *J. Pharm. Biomed. Anal.* **2016**, 120, 65, DOI: 10.1016/j.jpba.2015.11.037.
18. Elshanawane A. A.; Abdelaziz L. M.; Hafez H. M. *Pharmaceut. Anal. Acta*. **2012**, 3, 175, DOI: 10.4172/2153-2435.1000175.
19. Tsutsumi, T.; Akiyama, H.; Demizu, Y.; Uchiyama, N.; Masada, S.; Tsuji, G.; Arai, R.; Abe, Y.; Hakamatsuka, T.; Izutsu, K.; Goda, Y.; Okuda, H. *Biol. Pharm. Bull*. **2019**, 42, 547, DOI: 10.1248/bpb.b19-00006.
20. Parr, M. K.; Joseph, J. F. *J. Pharm. Biomed. Anal*. **2019,** 64, 536, DOI: 10.1016/j.jpba.2018.11.010.
21. The European Directorate for the Quality of Medicines & HealthCare (EDQM), *Method for the determination of NDMA and NDEA by LC-MS/MS in Sartan containing film coated tablets*. Available at: https://www.edqm.eu/sites/default/files/method_for_the_determination_of_ndma_and_ndea_by_lc-ms-ms_in_sartan_containing_film_coated_tablets.pdf. Published 2019. Accessed December 1, 2020.
22. Chang, S. H.; Chang, C. C.; Wang, L. J.; Chen, W. C.; Fan, S. Y.; Zang, C. Z.; Hsu, Y. H.; Lin, M. C.; Tseng, S. H.; Wang, D. Y. *J. Food Drug Anal*. **2020**, 28, 2. DOI: 10.38212/2224-6614.1063.
23. Chen, W.; Li, X; Huang, H; Zhu, X; Jiang, X; Zhang, Y; Cen, K; Zhao, L; Liu, X; Qi, S. *Chemosphere* **2017**, 168, 1400, DOI: 10.1016/j.chemosphere.2016.11.109.
24. United States Food and Drug Administration*, Combined N-Nitrosodimethylamine (NDMA) and N-Nitrosodiethylamine (NDEA) Impurity Assay by GC/MS-Headspace.* Available at: https://www.fda.gov/media/117843/download. Published 2019. Accessed December 1, 2020.
25. International Council for Harmonisation of Technical Requirements for Pharmaceuticals for Human Use (ICH), *Validation of analytical procedures: text and methodology, Q2(R1)*, ICH, **2005**.
26. Lee, J. H.; Lee, S. U.; Oh, J. E. *Int. J. Environ. Anal. Chem.* **2013**, 12, 126, DOI: 10.1080/03067319.2013.803281.
27. Santillana, M. L.; Bustos, J; Nieto, M. T. *Revista Del Comité Científico de la AECOSAN* **2018**, 27, 95.
28. United States Food and Drug Administration (FDA), *GC/MS Headspace Method for Detection of NDMA in Valsartan Drug Substance and Drug Products*, FDA, Available at: https://www.fda.gov/media/115965/download.
29. United States Food and Drug Administration (FDA), *Combined direct injection N-nitrosodimethylamine (NDMA), N-nitrosodiethylamine (NDEA), N-nitrosoethylisopropylamine (NEIPA), N-nitrosodiisopropylamine (NDIPA), and N-nitrosodibutylamine (NDBA) impurity assay by GC-MS/MS*, FDA, Available at: https://www.fda.gov/media/123409/download.
30. Health Canada, *Impurities found in certain angiotensin II receptor blocker (ARB) products, also known as sartans*. Health Canada, Available at: https://www.canada.ca/en/health-canada/services/drugs-health-products/compliance-enforcement/information-health-product/drugs/angiotensin-receptor-blocker.html.

Vol. 12, No. 2, 2021
ISSN 2233-4203/ e-ISSN 2093-8950
ARTICLE
www.msletters.org | Mass Spectrometry Letters

Statistical Characterization of the Multi-Charged Fragment Ions in the CID and HCD Spectrum

Sangeetha Ramachandran[1]* and Tessamma Thomas[2]

[1]*Department of Electronics, Cochin University of Science and Technology, Cochin-682022, Kerala, India*
[2]*Department of Electronics, Cochin University of Science and Technology, Cochin-682022, Kerala, India*

Received in March 7, 2021; Revised May 24, 2021; Accepted May 27, 2021
First published on the web June 30, 2021; DOI: 10.5478/MSL.2021.12.2.41

Abstract : Collision-induced dissociation (CID) and higher-energy collisional dissociation (HCD) are the widely used fragmentation technique in mass spectrometry-based proteomics studies. Understanding the fragmentation pattern from the tandem mass spectra using statistical methods helps to implement efficient spectrum analysis algorithms. The study characterizes the frequency of occurrence of multi-charged fragment ions and their neutral loss events of doubly and triply charged peptides in the CID and HCD spectrum. The dependency of the length of the fragment ion on the occurrence of multi-charged fragment ion is characterized here. Study shows that the singly charged fragment ions are generally dominated in the doubly charged peptide spectrum. However, as the length of the product ion increases, the frequency of occurrence of charge 2 fragment ions increases. The y- ions have more tendencies to generate charge 2 fragment ions than b- ions, both in CID and HCD spectrum. The frequency of occurrence of charge 2 fragment ion peaks is prominent upon the dissociation of the triply charged peptides. For triply charged peptides, product ion of higher length occurred in multiple charge states in CID spectrum. The neutral loss peaks mostly exist in charge 2 states in the triply charged peptide spectrum. The b-ions peaks are observed in much less frequency than y-ions in HCD spectrum as the length of the fragment increases. Isotopic peaks are occurred in charge 2 state both in doubly and triply charged peptide's HCD spectrum.

Keywords : CID, HCD, fragmentation pattern, multi-charged ions, LC-MS/MS

Introduction

Tandem mass spectrometry (MS/MS) is the most widely used technology to characterize the peptides in the complex sample.[1] The proteins are digested into peptides and analyzed in MS1. The parent peptide ion isolated from MS1 is dissociated and analyzed in MS2. Different dissociation technique creates different patterns of fragmentation spectra. HCD and CID fragment the peptide at its amide bond along its peptide backbone generates predominantly N-terminal b-ions and C-terminal y-ions. The b- & y-type fragment ions can further fragment by losing small neutral molecules, creates neutral loss b- & y-ion peaks in the spectrum. The difference in collission energy in CID and HCD dissociation causes changes in their fragmentation spectra.

The basic theory of peptide fragmentation was first explained by Wysocki et al. in their mobile proton hypothesis.[2] The parent ion proton moves along the amide bond and cleaves its backbone at the most favorable point. Kapp et al.[3] proved that the mobility of charge is hindered by the basic residues within the peptide. The different fragmentation pathways are extensively investigated in the literature. The researchers have studied the fragmentation patterns using statistical analysis of the large set of data. The data mining and machine learning approaches were used to analyze the spectral pattern, which proves the residue-specific cleavage preferences of CID fragmentation pattern.[4–8] The statistical analysis of neutral loss events also proved the influence of residues in the fragmentation pattern. Most of the works are focused on the intensity information from the mass spectrum. Shao et al.[9] characterised the HCD and CID spectrum and found that the intensity of y- ions reached a maximum in the 60–70% and 40–50% relative mass bins of HCD spectra from doubly and triply charged peptides, respectively. The multi-charged fragment ions were analyzed based on the relative mass bins. Zubarev et.al[9] compared CID cleavage selectivity to ECD (electron capture dissociation). They found that the yn-2 (n refers to peptide length) fragment had the highest intensity of all y ions.

*Reprint requests to Sangeetha Ramachandran,
https://orcid.org/0000-0002-8033-294X
E-mail: sangeetharamachandran.25@gmail.com

Multi charged peptide dissociates into singly charged fragment ions, or the entire charge may retain on one fragment. The fragmentation of the doubly charged peptide generates singly and doubly charged fragment ions. Similarly, the fragmentation of triply charged peptides generates singly, doubly, and triply charged fragment ions. The x-axis of the tandem mass spectra has the mass/charge (*m/z*) value of fragment ion. The *m/z* of the doubly charged fragment ion will be nearly half of that of its singly charged fragment ion. Similarly mass of triply charged fragment ion will be nearly 1/3 of its singly charged fragment ion. Hence the generation of multi-charged fragment ions creates the more complex pattern in the tandem mass spectrum. For example, the CID spectrum of the doubly charged peptide 'DKGEAENEAKPIDVK' is shown in the Figure 1. The singly and doubly charged fragment ion y10 (y10+ & y10++) are appeared at *m/z* 251.11 & 571.80 respectively in CID spectrum. Not all fragment ions appeared in both charge states. Hence it is necessary to characterize the occurrence of multi charged fragment ions in the tandem mass spectrum for the reliable interpretation of the spectrum.

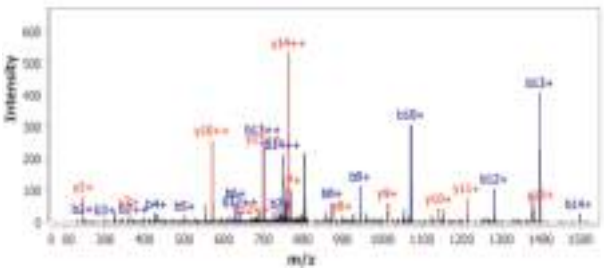

Figure 1. CID spectrum of the peptide 'DKGEAENEAKPIDVK'.

In this study, the frequency of occurrence of multi-charged fragment ions of doubly and triply charged peptides in HCD & CID spectra is analyzed. The dependency of the number of residues in the fragment is characterized here.

Method

Dataset

The CID spectrum of doubly and triply charged peptides were downloaded from the NIST human peptide spectral library (chemdata.nist.gov).[10] The spectral library provides high-quality reference consensus spectrum annotated with peptide for mass spectrometry-based proteomics studies. Dataset consists of 87661 and 29153 mass spectra of doubly & triply charged tryptic peptides, respectively, with no missed cleavage, and modifications are used for this study.

The HCD spectra of doubly and triply charged peptides were downloaded from ProteomeTool project spectral library.[11] It contains high-quality reference spectra of synthetic peptides of human proteome analyzed on LTQ Orbitrap fusion. Dataset consists of 188514 and 64087 mass spectra of doubly & triply charged tryptic peptides, respectively, with no missed cleavage and modifications are used for this study.

Methodology for analyzing multi-charged fragment ion peaks pattern

The relative frequency information was used to characterize the fragment ions and the neutral loss events in our previous studies.[12,13] Here also, the frequency of occurrence of fragment ion peaks is estimated to characterize the multi-charged fragment ion peaks in CID and HCD spectrum. The frequency statistics are calculated with respect to the length of the fragment ion or the position of the cleavage site along the length of the peptide. The maximum length of peptide considered in this study is 21. Hence the length of the fragment ion can vary from 1-20. The dataset contains large set of spectra of known sequences. From the peptide list, the possible number of times a particular ion b/y ion can be generated upon a cleavage position along the length of the peptide is estimated and is denoted as N^t_n. Here 't' denote fragment ion type b-/y- ion, 'n' denotes the number of residues in the fragment ion. From the CID & HCD spectra, the actual number of times an ion observed in the spectra is estimated and denoted as $C^t_{p,n}$. The frequency of occurrence of a fragment ion with respect to the length of the fragment is calculated using equation1.

$$F^t_p(n) = \frac{C^t_{p.n}}{N^t_n} \quad (1)$$

Where, p € { bn+, bn++, yn+, yn++ in case of doubly charged peptide spectrum
bn+, bn++, bn+++, yn+, yn++, yn+++ in case of triply charged peptide spectrum}

Here 'p' represents the singly and multi charged b- & y-ions comprising of the allied peaks of neutral losses and isotopic peaks. The study focused on the analysis of b- & y- ion peaks corresponding to the loss of nominal mass units: b/y- 17 (NH_3), 18 (H_2O), 34 (NH_3+NH_3), 35 (NH_3+ H_2O), 36 (H_2O + H_2O).

Results and Discussion

In our previous studies, we characterized the fragment ion peaks and their neutral loss peaks for the comprehensive understanding of the fragmentation pattern. The studies have proved the influence of residue-specific and position-specific cleavage preferences of CID fragmentation pattern.[12,13] The statistical features extracted were found to be consistent with the log-transformed intensity of the experimental spectrum. Hence, the features were efficiently

used to model the CID spectra and to identify the peptide from the CID spectra.[14,15] In this study, the frequency of occurrence of multi-charged fragment ions on CID and HCD spectra is characterized and compared. Shao et al. proved that the percentage of multi-charged fragment ions gradually increases with an increase in the relative mass of fragment.[9] The relative mass is the fragment ion mass divided by the precursor mass. In the triply charged peptide spectrum, the multi-charged fragment ions are prominent in the higher relative mass region. The dependency of the number of residues in the fragment ion is investigated in this study.

Characterization of multi-charged fragment ions in doubly charged peptide spectrum

The influence of the length of fragment ions for the generation of fragment ions in charge 2 states in the doubly charged peptide spectrum is characterized here. Initially, the fragment ions- b or y ions encompass all its allied peaks. The relative frequency of occurrence of charge one and two fragments of b- & y- ions plotted with respect to the length of fragment ion in CID and HCD spectrum are shown in Figure 2(a) and 2(b), respectively.

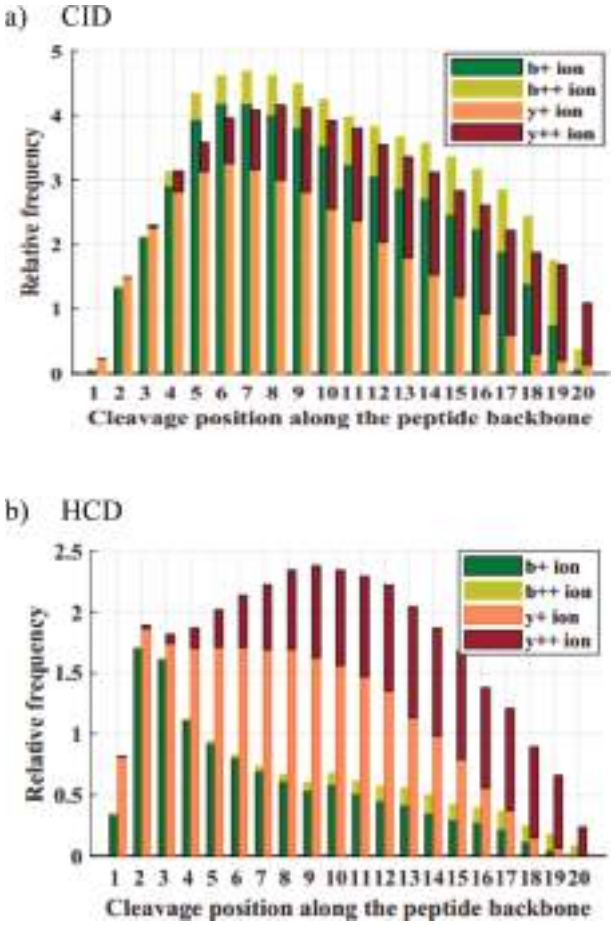

Figure 2. Charge state of fragment ions versus the length of the fragment. The relative frequency of occurrence of fragment ions b+, b++, y+, and y++ along the length of the peptide in CID and HCD spectrum is shown in Figure 2(a) and 2(b), respectively. The x-axis represents the length of the fragment ion. Y-axis represents the relative frequency of occurrence of fragment ion peaks.

Figure 2 shows that the occurrence of singly charged fragment ion peaks dominated in the doubly charged peptide's spectrum. The occurrence of charge 2 fragment ion peak increases as the length of the fragment ion increases. The y-ion has more tendencies to be in the y++ state. As the length of the fragment greater than 14, the frequency of occurrence of y++ ions are higher than the y+ ion. Compared to CID spectrum, HCD spectrum has the lesser frequency of occurrence of b-ion, and has very less b++ fragment ions. The frequency of occurrence of y-ions are higher in HCD spectrum as shown in Figure 2(b). Hence, it is inferred that, with the increase in length of the peptide, the frequency of occurrence of doubly charged fragment ion peaks in the CID & HCD spectrum increases. The b-ions peaks observed much less frequency than y-ion in HCD spectrum as the length of the fragment increases. This is because b-ions are less stable due to higher collision energy.[9]

Considering the neutral loss events and isotopic events in the CID & HCD spectrum of doubly charged peptides, the percentage of occurrence of charge 2 fragment ion of b- and y-type ion is shown in color map Figure 3(a) and 3(b), respectively. The color map emphasis how frequently the allied peaks of b-ion such as b-, b-isotopic, b-17, b-18, b-34, b-35, b-36, b-44, b-45, b-46, b+18 and y-ion such as y-, y-isotopic, y-17, y-18, y-34, y-35, y-36, y-44, y-45, y-46 occurred in charge 2 state as the length of fragment increases. The loss peak y-35 is not available in CID spectrum, hence not shown in colormap.

Figure 3 shows that as the length of the fragment increases, the neutral loss peaks are more frequently observed in charge 2 states. The loss of multiple neutral molecules, hence the generation of b-34, b-35, b-36, y-34, y-35, y-36 peaks more frequently observed in charge 2 state. In the case of y-ion, as the length of the fragment increases, the loss peaks of y-ions are frequently observed in charge 2 state. The isotopic peaks of b- & y-ions are frequently occurred in charge 1 state in CID spectrum, while in HCD spectrum, isotopic peaks mostly occur in charge 2 state in the doubly charged peptide's spectrum.

Characterization of multi-charged fragment ions in triply charged peptide spectrum

The influence of the length of the fragment for the generation of fragment ions in the charge 2 & 3 states in triply charged peptide spectrum is characterized here. The triply charged peptide undergoing fragmentation can generate singly, doubly, and triply charged fragment ions. The frequency of occurrence of b- & y- ions (encompassing its

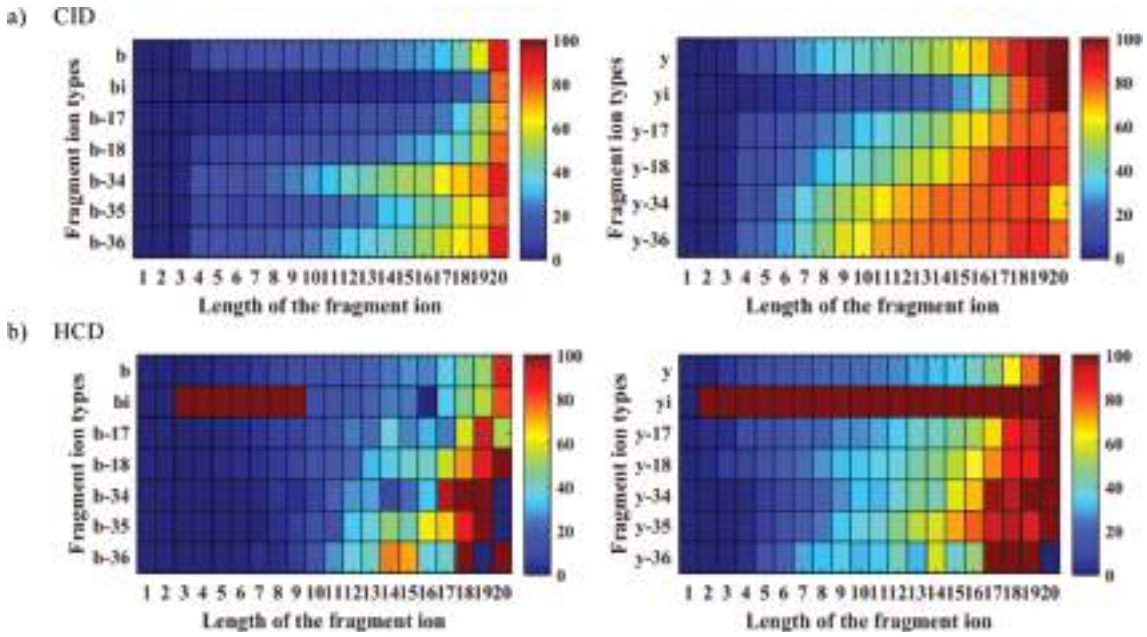

Figure 3. Percentage of occurrence of charge 2 state fragment ions among the fragment ion peaks. The x-axis represents the length of the fragment ion. Y-axis represents the allied peaks of b- & y-ions.

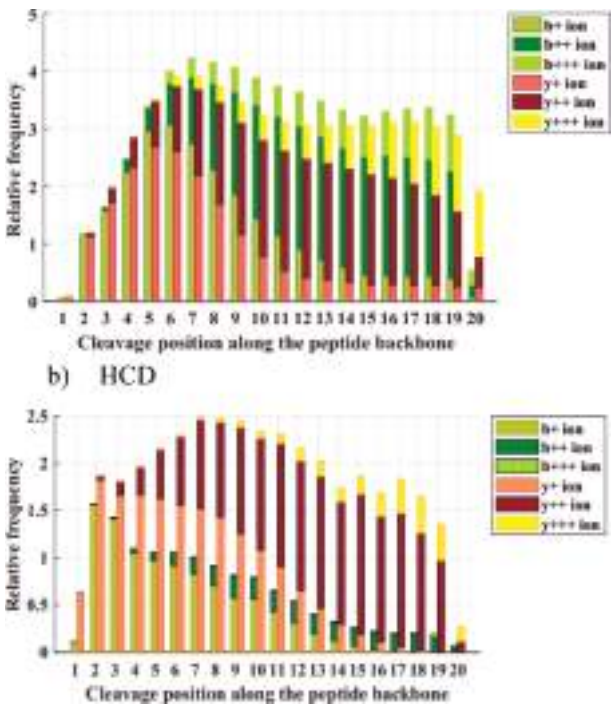

Figure 4. Charge state of fragment ions versus the length of the fragment. The figure shows the relative frequency of occurrence of fragment ions b+, b++, b+++, y+, y++, and y+++ along the length of the peptide. The x-axis represents the length of the fragment ion. Y-axis represents the relative frequency of occurrence of fragment ion peaks.

allied peaks) along the length of the peptide in charge 1, 2 & 3 states in CID and HCD spectrum are plotted in Figure 4(a) and 4(b) respectively.

From Figure 4(a) it is clear that, with the increase in the length of the fragment, the multi-charged fragment ion peaks are more frequently observed than singly charged fragment ion. Charge 2 fragment ion peaks are more prominent in the triply charged peptide spectrum. At higher length, the multiple charge state fragment ions are produced in the CID spectrum. In the HCD spectrum (Figure 4(b)), b-ions are observed in much less frequency as the length of the fragment ions increases. Singly charged b-ions are more frequently observed than the charge 2 state. Singly charged y-ions occurred in higher degree at lower length and y++ fragment ions dominated in the triply charged peptide's HCD spectrum as the length of the fragment ion increases.

Considering the neutral loss peaks and isotopic peaks in the CID & HCD spectrum of triply charged peptides, the percentage of occurrence of multi charged fragment ion of b- and y-type ion is plotted in the color map (Figure 5). Figure 5.i shows the percentage of occurrence of charge 2 b- & y- fragment ions and their allied peaks, respectively. Figure 5.ii shows the percentage of occurrence of charge 3 b- & y- fragment ions and their allied peaks, respectively.

The key results examined from the Figure 5 are discussed as follows. The frequency of occurrence of charge 2 fragment ion peaks is prominent upon the dissociation of triply charged peptides. The multi-charged neutral loss peaks increases as the length of the fragment ion increases. The neutral loss peaks of y-ions have more tendency to exist in

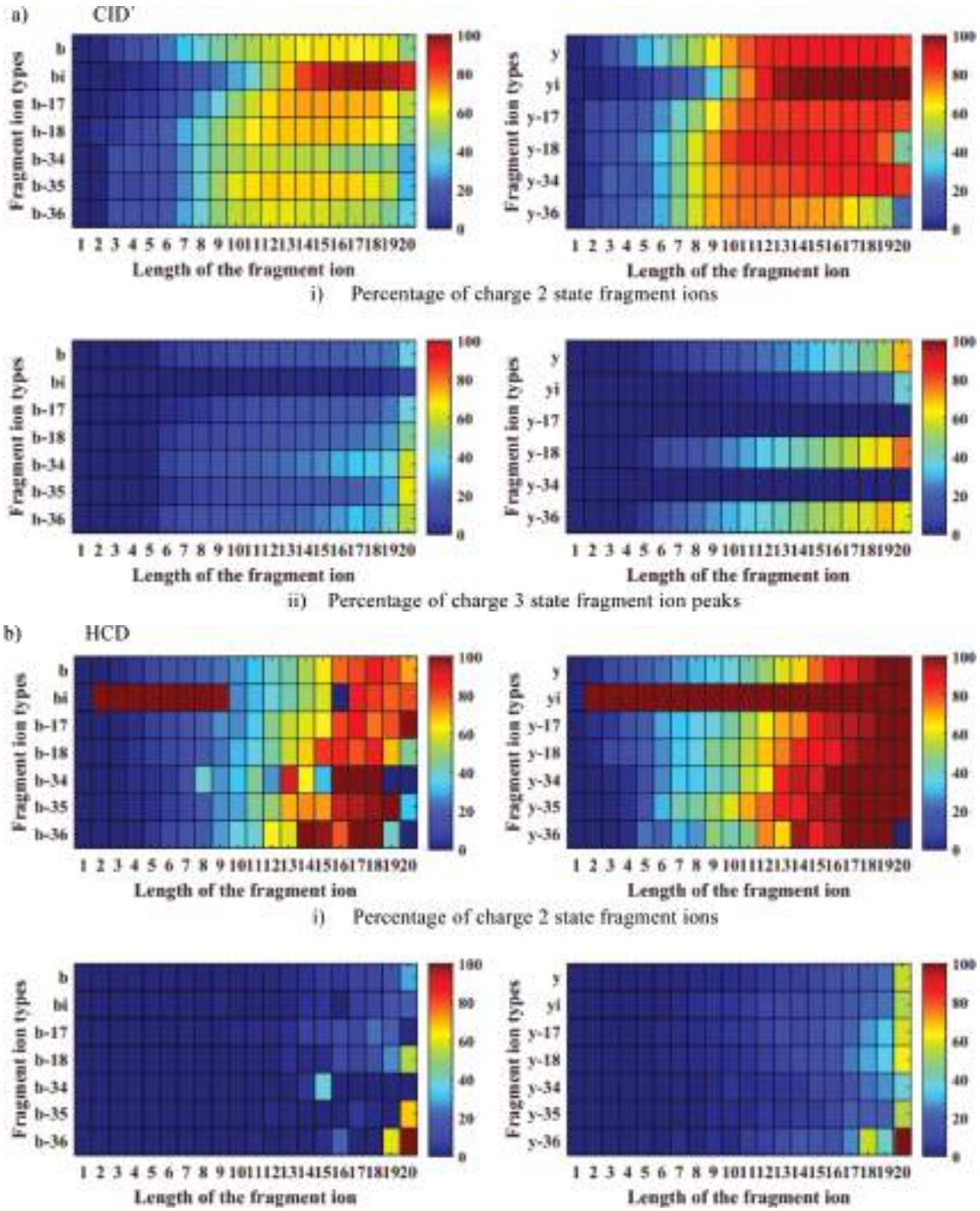

Figure 5. The percentage of occurrence of fragment ion peaks with charge 2 & 3 state. The x-axis represents the length of the fragment ion. Y-axis represents the allied peaks of b- & y-ions.

charge 2 state. The loss of water from y-ion (y-18 & y-36) has shown different patterns to exist in charge 3 state in CID spectra. Hence it can be inferred that the charge 3 fragment ion of y-ion has more tendency to lose water from its ions. Dissociation of a triply charged peptide is more likely to generate doubly charged isotopic peaks than the singly and triply charged isotopic peaks of b- & y- ions. In CID spectra, doubly charged isotopic peaks prominent in higher length fragment ion, while in HCD spectra, doubly charged isotopic peaks are prominent from lower length.

Conclusions

The occurrences of multi-charged fragment ions in the tandem mass spectrum add more complexity to the spectrum, hence the reliable interpretation of peptide sequence from the spectrum. The relative frequency of occurrence of multi-charged fragment ions in the doubly and triply charged peptide spectrum is studied here. Study shows that the singly charged fragment ions are generally dominated in the doubly charged peptide CID & HCD spectrum. However, as the length of the product ion increases, the frequency of occurrence of charge 2 fragment ions increases. The y- ions have more tendencies to generate charge 2 fragment ions than b- ions. In HCD spectrum, the relative frequency of occurrence of b-ions are much lesser than y-ion as the length of the fragment ion increases. The consecutive loss of ammonia and water from the y-ion occurs mostly from the doubly charged fragment ion y++. In the doubly charged peptide spectrum, isotopic peaks are more likely to occur in the singly charged state in CID spectrum and in the charge 2 state in HCD spectrum. For triply charged peptides, product ion of higher length occurred in multiple charge states. In both CID and HCD spectrum, isotopic peaks are more likely to occur in charge 2 state upon the dissociation of a triply charged peptide. Multi-charged neutral loss peaks gradually increases as the length of the fragment increases. Neutral loss from y-ions shows a higher tendency to exist in charge 2 state. In CID spectrum, the loss of water from y-ion (y-18 & y-36) has shown different patterns to exist in charge 3 state. Thus charge 3 fragment ion of y-ion has more tendency to lose water from its ions. The study provides the statistical trends of occurrence of fragment ion peaks in the mass spectrum, which helps in reliable interpretation of the peptide from the CID & HCD spectrum.

Acknowledgments

The authors would like to acknowledge the support from the Department of Electronics, Cochin University of Science and Technology.

References

1. Aebersold, R.; Mann, M. *Nature* **2003**, 422, 198, DOI: 10.1038/nature01511.
2. Wysocki, V. H.; Tsaprailis, G.; Smith, L. L.; Breci, L. A. *J. Mass Spectrom.* **2000**, 35, 1399, DOI: DOI: 10.1002/1096-9888(200012)35:12<1399::AID-JMS86>3.0.CO;2-R.
3. Kapp, E. A. Schütz, F.; Reid, G. E.; Eddes, J. S.; Moritz, R. L.; O'Hair, R. A. J.; Speed, T. P.; Simpson, R. J. *Anal. Chem.* **2000**, 75, 6251, DOI: 10.1021/ac034616t.
4. Tabb, D. L.; Smith, L. L.; Breci, L. A.; Wyscocki, V. H.; Lin, D.; Yates, J. R. *Anal. Chem.* **2003**, 75, 1155, DOI: 10.1021/ac026122m.
5. Huang, Y.; Triscari, J. M.; Tseng, G. C.; Pasa-Tolic, L,; Lipton, M. S.; Smith, R. D.; Wysocki, V. H. *Anal. Chem.* **2005**, **77**, 5800, DOI: 10.1021/ac0480949.
6. Huang, Y. Tseng, G. C.; Yuan, S.; Pasa-Tolic, L.; Lipton, M. S.; Smith, R. D.; Wysocki, V. H. *J. Proteome Res.* **2008**, 7, 70, DOI; 10.1021/pr070106u.
7. Loo, J. A.; Edmonds, C. G.; Smith, R. D. *Anal. Chem.* **1993**, 65, 425, DOI: 10.1021/ac00052a020.
8. Lau, K. W.; Hart, S. R.; Lynch, J. A.; Wong, S. C. C.; Hubbard, S. J.; Gaskell, S. J. *Rapid Commun. Mass Spectrom.* **2009**, 23, 1508, DOI: 10.1002/rcm.4032.
9. Shao, C.; Zhang, Y.; Sun, W. *J. Proteomics* **2014**, 109, 26, DOI: 10.1016/j.jprot.2014.06.012.
10. Stein, S. E.; Pudnick, P. A. *NIST Peptide Tandem Mass Spectral Libraries. Human Peptide Mass Spectral Reference Data*, National Institute of Standards and Technology: Gaithersburg, MD, **2008**, DOI: 10.18434/T4ZK5S.
11. Zolg, D. P.; Wilhelm, M.; Schnatbaum, K.; Zerweck, J.; Knaute, T.; Delanghe, D.; Bailey, D. J.; Gessulat, S.; Ehrlich, H.-C.; Weininger, M.; Yu, P.; Schlegl, J.; Kramer, K.; Schmidt, T.; Kusebauch, U.; Deutsch, E. W.; Aebersold, R.; Moritz, R. L.; Wenschuh, H.; Moehring, T.; Aiche, S.; Huhmer, A.; Reimer, U.; Kuster, B. *Nat. Methods* **2017**, 14, 259, DOI: 10.1038/nmeth.4153.
12. Ramachandran, S.; Thomas, T. **2019**, 10, 7, DOI: 10.5478/MSL.2019.10.2.50.
13. Ramachandran, S.; Thomas, T. *Int. J. Mass Spectrom.* **2020**, 448, 116270, DOI: 10.1016/j.ijms.2019.116270.
14. Ramachandran, S.; Thomas, T. A *ACS Omega* **2020**, 5, 12615, DOI: 10.1021/acsomega.9b03935.
15. Ramachandran, S.; Thomas, T. *J. Proteomics* **2021**, 235, 104116, DOI: 10.1016/j.jprot.2021.104116.

Vol. 12, No. 2, 2021
ISSN 2233-4203/ e-ISSN 2093-8950
ARTICLE
www.msletters.org | Mass Spectrometry Letters

Estimation of Phosphorus Concentration in Silicon Thin Film on Glass Using ToF-SIMS

M. Abul Hossion[1]*, Karthick Murukesan[2], and Brij M. Arora[3]

[1]*Department of Physics, Bangabandhu Sheikh Mujibur Rahman Maritime University, Dhaka 1216, Bangladesh*
[2]*Department of Electrical Engineering, University of Cambridge, Cambridge CB21PZ, United Kingdom*
[3]*Department of Physics, University of Mumbai, Mumbai 400098, India*

Received in May 26, 2021; Revised June 20, 2021; Accepted June 28, 2021
First published on the web June 30, 2021; DOI: 10.5478/MSL.2021.12.2.47

Abstract : Evaluating the impurity concentrations in semiconductor thin films using time of flight secondary ion mass spectrometry (ToF-SIMS) is an effective technique. The mass interference between isotopes and matrix element in data interpretation makes the process complex. In this study, we have investigated the doping concentration of phosphorus in, phosphorus doped silicon thin film on glass using ToF-SIMS in the dynamic mode of operation. To overcome the mass interference between phosphorus and silicon isotopes, the quantitative analysis of counts to concentration conversion was done following two routes, standard relative sensitivity factor (RSF) and SIMetric software estimation. Phosphorus doped silicon thin film of 180 nm was grown on glass substrate using hot wire chemical vapor deposition technique for possible applications in optoelectronic devices. Using ToF-SIMS, the phosphorus-31 isotopes were detected in the range of 10^1~10^4 counts. The silicon isotopes matrix element was measured from p-type silicon wafer from a separate measurement to avoid mass interference. For the both procedures, the phosphorus concentration versus depth profiles were plotted which agree with a percent difference of about 3% at 100 nm depth. The concentration of phosphorus in silicon was determined in the range of 10^{19}~10^{21} atoms/cm^3. The technique will be useful for estimating distributions of various dopants in the silicon thin film grown on glass using ToF-SIMS overcoming the mass interference between isotopes.

Keywords : ToF-SIMS, HWCVD, phosphorus, mass interference, RSF, thin film, glass

Introduction

An accurate quantification of the dopant profile in semiconductor is a complex task even today with the scaling down of devices such as, transistors[1] and thin film solar cell.[2] The dopants concentration in the semiconductor can be simulated using stopping and range of ions in matter (SRIM) computation code[3] from an ion implanted sample. For generalised samples, secondary ion mass spectrometry (SIMS) is widely used in the semiconductor material characterization.[4,5,6] The process allows the in-depth detection of various isotopes on the top or below the surface of a sample.[7] The mass interference between isotopes and matrix element makes the data interpretation process complex. Particularly, the detection of phosphorous in silicon suffers from the mass interference. The quantification of phosphorus or other dopant is critical for the performance of the electronics devices from various processes, such as, metal organic vapor phase epitaxy (MOVPE),[8] atomic layer deposition (ALD)[9] and chemical vapour deposition (CVD).[10] The analysis of phosphorus in the silicon thin films were executed in a high mass resolution ($m/\Delta m>10000$)[11] magnetic sector SIMS to separate phosphorus-31 (^{31}P) and hydrogenated silicon ($^{30}Si^1H$) isotopes.[12] The magnetic sector SIMS such as IMS-6f from Cameca, France, was used to eliminate the mass interference during data acquisition.[13,14] In the years 2010-2020, time of flight (ToF) SIMS is being widely used in academia due to its high sensitivity to trace elements, two dimensional elemental mapping (imaging) capacity, surface analysis of insulating/conducting material and the depth profiling at nano meter scale.[15] High depth resolution ToF-SIMS with charge compensation has also been used to examine secondary ion depth profiles relative to P and Si elements.[16]

In this article, phosphorus doped silicon thin film of 180 nm was grown on glass substrate using hot wire chemical vapor deposition (HWCVD) technique for possible applications in optoelectronic devices. The phosphorus

Open Access
*Reprint requests to M. Abul Hossion,
https://orcid.org/0000-0002-3199-1682
E-mail: abulhossion.phy@bsmrmu.edu.bd

Table 1. Veeco Dektak 150 surface profiler data for the crater depth and the scanning length.

Sample name	Cursor position	Cursor width (mm)	X-axis position (mm)	Crater length (mm)	Y-axis position (nm)	Crater depth (nm)
Reference phosphorus	Left	0.08	0.1534	0.9028	0.9088	1137.18
	Middle	0.08	0.6049		-1093.40	
87-nSi-Glass	Right	0.08	0.9103	0.8764	0.6210	242.45
	Middle	0.08	0.4721		-243.31	

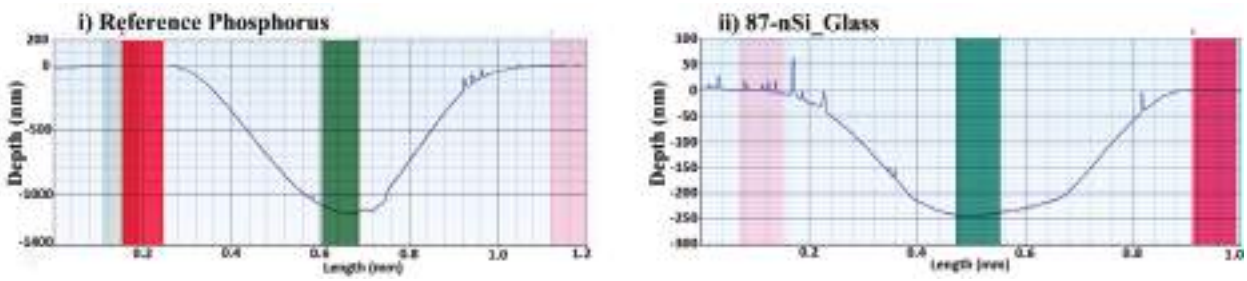

Figure 1. The total depth of the crater for i) reference phosphorus diffused silicon wafer is 1137.18 nm and for ii) 87-nSi-Glass phosphorus doped silicon thin film using HWCVD on glass is 242.45 nm measured using the Veeco Dektak 150 surface profiler.

concentration in the hydrogenated silicon thin film on glass was evaluated by ToF-SIMS using dynamic mode of operation. To avoid the mass interference, only ^{31}P isotope in silicon was measured. The matrix elements of silicon isotopes (^{30}Si, $^{30}Si^{1}H$) were detected in separate measurements. The quantitative analysis of counts to concentration conversion was done following two routes, standard relative sensitivity factor (RSF) with the silicon matrix element and SIMetric software (SW) estimation from reference sample without the silicon matrix element.

Experimental

Sample Preparation

Three samples were studied in this work. i) The phosphorus doped microcrystalline silicon thin films were grown on glass substrate using gas flow ratio of SiH_4:H_2:PH_3 = 2:50:1 sccm as an emitter layer in p-i-n diode[17]. The thin silicon film was synthesized by HWCVD technique at 350°C substrate temperature with a tantalum filament kept at a temperature of 1650°C.[18] The growth duration was 45 min for 180 nm thin film.[19] ii) An infrared laser from single emitter diode source with wavelength 1064 nm by SPI lasers limited, Germany was used to anneal the phosphorus doped silicon film on glass.[20] iii) The reference phosphorous sample was prepared in a diffusion furnace at 890°C for 15 min on 2 inch diameter n-type silicon wafer.[21] This diffusion process allows the phosphorus atoms to diffuse at about 600 nm.

Depth Profile analysis

The total crater depth was measured using the Veeco Dektak 150 surface profiler and the corresponding data is given in Figure 1 and Table 1. The sputtering rate for the Reference phosphorus diffused silicon wafer is 0.28 nm/s, where the crater depth is 1137.2 nm as shown in Figure 1(i) and total sputtering duration is 4020 s. The sputtering rate for 87-nSi-Glass phosphorus doped silicon thin film on glass using HWCVD is 0.30 nm/s, where the total crater depth is 242.5 nm as shown in Figure 1(ii) and total sputtering duration is 820 s.

ToF-SIMS data acquisition

To measure the secondary ion counts, the PHI nano ToF II TRIFT was used from Physical Electronics, MN, USA. In this process, a 10 ns pulsed liquid metal ion gun (LMIG) uses Gallium (Ga^+) sources to produce ions as primary ion beam to ionise the surface molecules.[22] The beam energy was kept 30 kV with a beam current of 15 nA and the raster size 300 × 300 μm^2.[23] The caesium ion (Cs^+) gun was used as sputtering tool to produce the negative secondary ions.[24] In the literature, dual beam IONTOF IV from Germany was used to profile phosphorus concentration with the Ga^+ ion gun at 25 kV, 1 pA for analysis and the Cs^+ ion gun at 1 kV, 80 nA for sputtering in the negative mode of operation.[25] In this study, the phosphorus isotope (^{31}P) was detected as secondary ions. The silicon isotope (^{30}Si) as the matrix elements were detected in a separate measurement from a p-type silicon wafer.[26] The ^{30}Si isotope counts was measured independently to avoid mass interference as well as to enhance the signal intensity.[27] The optimized scanning parameters for better depth resolution and improved detection limit are given in the Table 2.

Table 2. ToF-SIMS scanning parameters for the detection of phosphorus isotope (^{31}P) in silicon thin film using caesium ion (Cs^+) sputtering gun.

Sample Name	Phosphorus thin film thickness (nm)	Sputtering beam current (A)	Sputtering beam energy (kV)	Sputtering beam raster area (μm^2)	Sputtering duration (s)	Mass analyser analysing duration (s)
408-Reference phosphorus	1000					
421-87-nSi-Glass	180	8.23×10^{-8}	3	300 × 300	20	60
422-87-nSi-Glass-Laser	180					

Table 3. Part of the data for the conversion of ToF-SIMS counts to concentration-depth profile. The complete data set is provided as supportive material.

Crater depth [Cycle number × Sputtering Duration (s) × Sputtering rate (nm/s)] (nm)	Measured intensity of ^{31}P isotope (counts)	Measured intensity of ^{30}Si in p-type silicon wafer[26] (counts)	Phosphorus concentration (using Eq. 1) (atoms/cm^3)	Phosphorus concentration SIMetric SW estimation (using Eq. 2) (atoms/cm^3)	Percent difference (%)
i) 408-Reference phosphorus diffused silicon wafer					
5.66	3023	33616	3.07E+20	2.29E+20	29
11.32	2884	46138	2.13E+20	2.18E+20	2
16.97	2913	47072	*2.11E+20	**2.20E+20	4
ii) 421-87-nSi-Glass phosphorus doped silicon thin film on glass using HWCVD					
5.91	7947	33616	8.06E+20	6.01E+20	29
11.83	5800	46138	4.29E+20	4.38E+20	2
17.74	5192	47072	3.76E+20	3.93E+20	4
iii) 422-87-nSi-Glass-Laser phosphorus doped silicon thin film on glass using HWCVD					
5.91	10924	33616	1.11E+21	8.26E+20	29
11.83	15561	46138	1.15E+21	1.18E+21	2
17.74	15866	47072	1.15E+21	1.20E+21	4

*Using equation 1, $C_B = 1.1 \times 10^{23} \times 0.031 \times (\frac{2913}{47072}) = 2.11 \times 10^{20}$ atoms/cm^3

** Using equation 2, $C_B = 7.56 \times 10^{16} \times 2913 = 2.2 \times 10^{20}$ atoms/cm^3

Results and Discussion

The ToF-SIMS signal is interpreted using relative sensitivity factor for Phosphorus Counts to concentration conversion. The concentration of phosphorus (C_P) in silicon is calculated using the following equations; equation 1 using the silicon matrix element and equation 2 without the matrix element,[4]

$$C_P = RSF_{P(Si)} \times \%^{30}Si \times \left(\frac{I_{P(Si)}}{I_{30Si}}\right) \quad (1)$$

$$C_P = RSF_{P(Si).EST.} \times I_{P(Si)} \quad (2)$$

Here, C_P is Concentration of phosphorus in silicon, $RSF_{P(Si)}$ is the relative sensitivity factor of phosphorus in silicon,[28] $\%^{30}Si$ is the fractional isotope abundance of ^{30}Si isotope in silicon,[29] $I_{P(Si)}$ is the intensity of phosphorus isotope (^{31}P) counts using Cs^+ gun, I_{30Si} is the intensity of silicon isotope (^{30}Si) counts on a p-type silicon wafer[26] using ToF-SIMS and $RSF_{P(Si).EST.}$ is the relative sensitivity factor of phosphorus in silicon estimated using SIMetric SW peak fitting tool from the 408-Rreference phosphorus diffused silicon wafer. Table 3 shows the part of data used in the phosphorus counts to concentration conversion calculation. The complete data table is provided with the article as supplementary material.

The Table 3 is used to plot phosphorus concentration versus crater depth curve for the i) Reference Phosphorus, ii) 87-nSi-Glass and iii) 87-nSi-Glass-Laser as shown in Figure 2 and 3 respectively. Figure 2 shows the concentration of phosphorus, diffused in n-type silicon wafer for Reference Phosphorus sample along with the SIMetric SW estimated curve. The concentration of phosphorus at the top surface of the silicon wafer is 2×10^{20} atoms/cm^3, which is in agreement with the value 4.3×10^{20} atoms/cm^3 obtained using CAMECA SC Ultra high resolution SIMS by Beljakowa et al..[9] Figure 3 shows the concentration of phosphorus in (i) 180 nm microcrystalline silicon thin film grown on glass using HWCVD and (ii) infrared laser (1064 nm) annealed micro crystalline silicon thin film grown on glass using HWCVD along with the corresponding SIMetric SW estimated curve respectively. From Figure

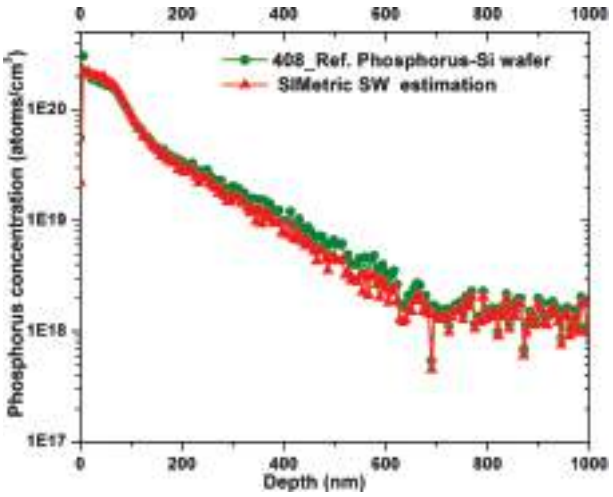

Figure 2. Phosphorus concentration – depth curve of sample 408_Ref.Phosphorus-Si wafer.

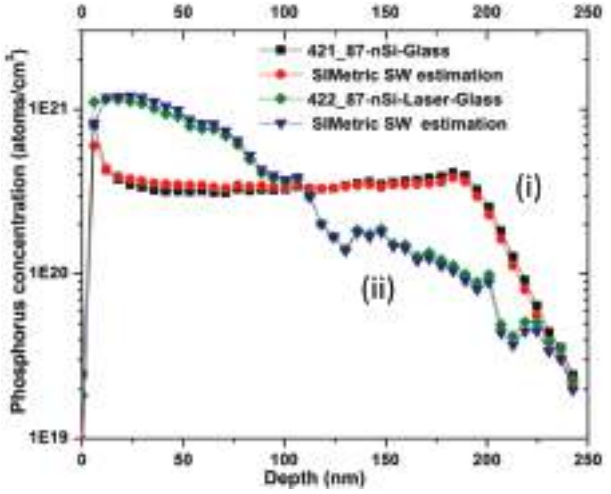

Figure 3. Phosphorus concentration – depth curve of sample (i) 421_87-nSi-Glass, and (ii) 422_87-nSi-Laser-Glass.

3(i), the concentration of phosphorus thin film is 3.25×10^{20} atoms/cm^3 at the top and this remain uniform over the top 180 nm. The Figure 3(ii) shows that, the laser irradiation caused significant changes in the thin film. It is seen that after the laser irradiation, the phosphorus concentration is no longer uniform. It has increased to 1.2×10^{21} atoms/cm^3 near the surface of the sample and decreased along the film thickness. This non-homogeneous laser absorption of silicon thin film is characterised using Raman imaging which is published elsewhere.[30] Furthermore, with laser irradiation, the silicon film melts and then starts to solidify from the position closest to the glass substrate. So, the film at the top surface solidifies later. The phosphorus has a segregation coefficient of around 0.35 which leads to an increase in the phosphorus concentration at the top surface as the top portion solidifies first.[31,32] The phosphorus concentration versus depth profiles of the RSF calculated and the SIMetric SW estimated are in agreement with a percent difference of about 3% at 100 nm depth, 12% at 200 nm, 20% 300 nm and 25% at 400 nm.

Conclusion

The concentration of phosphorus in silicon thin film grown on glass using HWCVD was estimated using ToF-SIMS technique in dynamic mode of operation. A phosphorus diffused silicon wafer was used as reference sample. The relative sensitivity factor along with silicon matrix element was used to interpret the ToF-SIMS data for each sample. Using SIMetric SW peak fitting tool, with the reference sample, the RSF was determined without the silicon matrix element data. The phosphorus counts to concentration conversion was performed using two routes, calculated RSF with silicon matrix element and simulated RSF procedure from reference sample. For the both procedures, the phosphorus concentration versus depth profiles were plotted which agree with a percent difference of about 3% at 100 nm depth. The concentration of phosphorus in silicon was determined in the range of 10^{19}~10^{21} atoms/cm^3 which is comparable with the value obtained using magnetic sector high resolution SIMS. The phosphorus in silicon detected on the top surface of phosphorus doped silicon thin film on glass was 3.25×10^{20} atoms/cm^3. The results of this study will be useful for the detection and quantification of impurities in wide area of thin films using ToF-SIMS technique overcoming the mass interferences between isotopes.

Acknowledgement

The authors thank, Jürgen Weippert, Fraunhofer Institute for Applied Solid State Physics, Freiburg, Germany, for the suggestions in data interpretation. The authors also thank, Dr. C. S. Harendranath, Principle research scientist, Sophisticated analytical instrument facility, Indian Institute of Technology Bombay, Mumbai, India, for providing ToF-SIMS laboratory facilities. The authors are grateful to Mr. Subhash Lokhre and Mr. Nilesh Marle for their active participation during the measurement process. We are grateful to HWCVD system team, Dr. Rajiv O. Dusane and Dr. Nilesh Wadibhasme, from the Department of Metallurgical Engineering and Materials Science, Indian Institute of Technology Bombay, Mumbai, India. We are also grateful to National Centre for Photovoltaic Research and Education (NCPRE) for allowing us to use the laser annealing tool.

Author Contributions

The authors Abul Hossion (A.H) and Brij Mohan Arora (B.M.A) participated in the conceptualization, designing

methodology, analysis, interpretation, discussion and improvement of the manuscript of the experimental data on ToF-SIMS study on phosphorus doped silicon film. Karthick Murukesan (K.M) prepared the reference sample and participated in the interpretation of SIMS data. A.H collected and analysed the data followed by the manuscript preparation while B.M.A does the review, editing, supervision and funding acquisition. All the figures and images are prepared by A.H. All the authors have read and agreed to this version of the manuscript.

Funding

This research was funded by Centre of Excellence in Nano electronics (CEN) of the Indian Institute of Technology, Bombay, Mumbai, India.

Conflicts of Interest

The authors declare no conflict of interest. The funders had no role in the design of the study; in the collection, analysis, or interpretation of data; in the writing of the manuscript, or in the decision to publish the results.

Supplementary Information

Supplementary information is available at https://drive.google.com/file/d/1TGFndqfANq9wCcfVK9HT3XT8J5fJF3ya/view?usp=sharing.

References

1. Yeoh, W. K.; Hung, S.-W.; Chen, S.-C.; Lin, Y.-H.; Lee, J. J. *Surf. Interface Anal*. **2020,** 52, 318, DOI: 10.1002/sia.6706.
2. Chen, H.-L.; Cattoni, A.; de Lépinau, R.; Walker, A. W.; Höhn, O.; Lackner, D.; Siefer, G.; Faustini, M.; Vandamme, N.; Goffard, J.; Behaghel, B.; Dupuis, C.; Bardou, N.; Dimroth, F.; Collin, S. *Nat. Energy* **2019,** 4, 761, DOI: 10.1038/s41560-019-0434-y.
3. Nipoti, R.; Parisini, A.; Boldrini, V.; Vantaggio, S.; Gorni, M.; Canino, M.; Pizzochero, G.; Camarda, M.; Woerle, J.; Grossner, U. *Mater. Sci. Forum* **2020,** 1004, 698, DOI: 10.4028/www.scientific.net/MSF.1004.698.
4. van der Heide, P. *Secondary Ion Mass Spectrometry: An Introduction to Principles and Practices*, *1st ed*. Wiley & Sons: New York, **2014**.
5. Riviere, J. C.; Myhra, S.; Myhra, S. *Handbook of Surface and Interface Analysis: Methods for Problem-Solving, 2nd Ed*. CRC Press: New York, **2009,** DOI: 10.1201/9781420007800.
6. Wilson, R. G. *Secondary Ion Mass Spectrometry: a Practical Handbook for Depth Profiling and Bulk Impurity Analysis*. Wiley & Sons: New York, **1989**.
7. Benninghoven, A.; Rudenauer, F. G.; Werner, H. W. *Secondary Ion Mass Spectrometry: Basic Concepts, Instrumental Aspects, Applications and Trends,* Wiley & Sons: New York, **1987**.
8. García-Tabarés, E.; Martín, D.; García, I.; Rey-Stolle, I. *Sol. Energy Mater. Sol. Cells* **2013,** 116, 61, DOI: 10.1016/j.solmat.2013.04.003.
9. Beljakowa, S.; Pichler, P.; Kalkofen, B.; Hübner, R. *Phys. Status Solidi A* **2019,** 216, 1900306. DOI: 10.1002/pssa.201900306.
10. Engelhardt, J.; Kromer, H.; Hahn, G.; Terheiden, B. AIP Conf. Proc. **2019,** 2147, 070002. DOI: 10.1063/1.5123863.
11. Maharrey, S.; Bastasz, R.; Behrens, R.; Highley, A.; Hoffer, S.; Kruppa, G.; Whaley, J. *Appl. Surf. Sci.* **2004,** 231–232, 972, DOI: 10.1016/j.apsusc.2004.03.197.
12. Li, Y.; Wang, S.; Lin, X.-F.; Wei, L. *Mater. Res. Soc. Symp. Proc.* **2005,** 862, 183, DOI: 10.1557/PROC-862-A18.3.
13. Loesing, R.; Guryanov, G. M.; Hunter, J. L.; Griffis, D. P. *J. Vac. Sci. Technol. B* **2000,** 18, 509, DOI: 10.1116/1.591222.
14. Hervig, R. L.; Mazdab, F. K.; Williams, P.; Guan, Y.; Huss, G. R.; Leshin, L. A. *Chem. Geol.* **2006,** 227, 83, DOI: 10.1016/j.chemgeo.2005.09.008.
15. Guilhaus, M. *J. Mass Spectrom.* **1995**, 30, 1519, DOI: 10.1002/jms.1190301102.
16. Mastromatteo, M.; Arduca, E.; Napolitani, E.; Nicotra, G.; Salvador, D. D.; Bacci, L.; Frascaroli, J.; Seguini, G.; Scuderi, M.; Impellizzeri, G.; Spinella, C.; Perego, M.; Carnera, A. *Surf. Interface Anal*. **2014,** 46, 393, DOI: 10.1002/sia.5578.
17. Hossion, A.; Khatavkar, S.; Arora, B. M. *J. Optoelectron. Adv. Mater.* **2021,** 23, 145.
18. Agarwal, M.; Pawar, A.; Wadibhasme, N.; Dusane, R. *Sol. Energy* **2017,** 144, 417, DOI: 10.1016/j.solener.2017.01.039.
19. Hossion, M. A.; Mondal, S.; Arora, B. M. *J. Russ. Laser Res.* **2020,** 41, 552, DOI: 10.1007/s10946-020-09910-9.
20. Mondal, S.; Solanki, C. S. *Mater. Sci. Semicond. Process*. **2017,** 59, 10, DOI: 10.1016/j.mssp.2016.11.011.
21. Murukesan, K.; Kumbhar, S.; Kapoor, A. K.; Dhaul, A.; Saravanan, S.; Pinto, R.; Arora, B. M. *$POCl_3$ Diffusion Process Optimization for the Formation of Emitters in the Crystalline Silicon Solar Cells; 2014 IEEE 40th Photovoltaic Specialist Conference (PVSC),* Denver (USA), 8-13 June 2014, p 3011, DOI: 10.1109/PVSC.2014.6925567.
22. Bayly, A. R.; Waugh, A. R.; Anderson, K. *Nucl. Instrum. Methods Phys. Res*. **1983**, 218, 375, DOI: 10.1016/0167-5087(83)91009-8.
23. Kia, A. M.; Haufe, N.; Esmaeili, S.; Mart, C.; Utriainen, M.; Puurunen, R. L.; Weinreich, W. *Nanomaterials* **2019,** 9, 1035, DOI: 10.3390/nano9071035.
24. Magee, C. W. *J. Electrochem. Soc*. **1979,** 126, 660, DOI: 10.1149/1.2129104.
25. Perego, M.; Caruso, F.; Seguini, G.; Arduca, E.; Mantovan, R.; Sparnacci, K.; Laus, M. *J. Mater. Chem. C*

2020, 8, 10229, DOI: 10.1039/D0TC01856B.
26. Hossion, M. A.; Arora, B. M. *Mass Spectrom. Lett.* **2021,** 12, 26, DOI: 10.5478/MSL.2021.12.1.26.
27. Stephan, T. *Planet. Space Sci.* **2001,** 49, 859, DOI: 10.1016/S0032-0633(01)00037-X.
28. Stevie, F. *Secondary Ion Mass Spectrometry: Applications for Depth Profiling and Surface Characterization*. Momentum Press: New York, **2015**.
29. Meija, J.; Coplen, T. B.; Berglund, M.; Brand, W. A.; Bièvre, P. D.; Gröning, M.; Holden, N. E.; Irrgeher, J.; Loss, R. D.; Walczyk, T.; Prohaska, T. *Pure Appl. Chem.* 2016, 88, 265, DOI: 10.1515/pac-2015-0305.
30. Hossion, A.; Maliakkal, C. B.; Mahmood, Z. H.; Arora, B. M. *Raman analysis of intrinsic and laser annealed n-type silicon film grown on glass using hot wire chemical vapor deposition; 2018 4th International Conference on Electrical Engineering and Information Communication Technology (ICEEiCT)*, Dhaka (Bangladesh) 13-15 September 2018, p 182, DOI:10.1109/CEEICT.2018.8628133.
31. Oberbeck, L.; Curson, N. J.; Hallam, T.; Simmons, M. Y.; Bilger, G.; Clark, R. G. *Appl. Phys. Lett.* **2004,** 85, 1359, DOI: 10.1063/1.1784881.
32. Nakano, S.; Liu, X.; Han, X.-F.; Kakimoto, K. *Crystals* **2021,** 11, 27, DOI: 10.3390/cryst11010027.

Vol. 12, No. 2, 2021
ISSN 2233-4203/ e-ISSN 2093-8950
ARTICLE
www.msletters.org | Mass Spectrometry Letters

Effect of Ginsenoside Rc on the Pharmacokinetics of Mycophenolic Acid, a UGT1A9 Substrate, and its Glucuronide Metabolite in Rats

So-Young Park[#], Ji-Hyeon Jeon[#], Su-Nyeong Jang, Im-Sook Song, and Kwang-Hyeon Liu*

BK21 FOUR Community-Based Intelligent Novel Drug Discovery Education Unit, College of Pharmacy and Research Institute of Pharmaceutical Sciences, Kyungpook National University; Daegu 41566, Korea

Received June 2, 2021; Revised June 28, 2021; Accepted June 30, 2021
First published on the web June 30, 2021; DOI: 10.5478/MSL.2021.12.2.53

Abstract : Previous *in vitro* studies have demonstrated that ginsenoside Rc inhibits UGT1A9, but there are no available data to indicate that ginsenoside Rc inhibits UGT1A9 *in vivo*. The effect of single and repeated intravenous injection of ginsenoside Rc was evaluated on the pharmacokinetics of mycophenolic acid. After injection of ginsenoside Rc (5 mg/kg for one day or 3 mg/kg for five days), 2-mg mycophenolic acid was intravenously injected, and the pharmacokinetics of mycophenolic acid and mycophenolic acid-β-glucuronide were determined. Concentrations of mycophenolic acid and its metabolite from rat plasma were analyzed using a liquid chromatography-triple quadrupole mass spectrometry. Single or repeated pretreatment with ginsenoside Rc had no significant effects on the pharmacokinetics of mycophenolic acid ($P > 0.05$): The mean difference in maximum plasma concentration (C_{max}) and area under the concentration-time curve (AUC_{inf}) were within 0.83- and 0.62-fold, respectively, compared with those in the absence of the ginsenoside Rc. These results indicate that ginsenoside Rc has a negligible effect on the disposition of mycophenolic acid *in vivo* despite *in vitro* findings indicating that ginsenoside Rc is a selective UGT1A9 inhibitor. As a result, ginsenoside Rc has little possibility of interacting with drugs that are metabolized by UGT1A9, including mycophenolic acid.

Keywords : Ginsenoside Rc, herb-drug interaction, mycophenolic acid, UGT1A9, uridine 5'-diphosphoglucuronosyltransferase

Introduction

Ginseng is a commonly used herbal medicine in Korea and other East Asian countries mainly due to its vitality restoration and immune-stimulating effect.[1-3] It has been increasingly consumed as a dietary supplement in many countries.[4-6] Formulations of ginseng extract are commonly used over-the-counter preparation in several countries, including Korea and the U.S.A. Processed ginseng products are estimated to be approximat ely US $2,085 million in the world market in 2009.[7] Many studies have shown that most of the pharmacological effects of ginseng are attributable to ginsenosides.[8] Ginsenosides have been known to have beneficial effects in diabetes,[9] dyslipidemia,[10] inflammatory diseases,[11] and cancer.[12]

Among various ginsenosides, ginsenoside Rc has antidiabetic, antiallergic, anticancer, and sedative effects.[13,14] Ginsenoside Rc is the second most abundant ginsenoside in commercially available red ginseng products.[15] Our previous study reported that ginsenoside Rc (Figure 1a) can inhibit UGT1A9 noncompetitively.[16] Ginsenoside Rc selectively inhibited UGT1A9-mediated mycophenolic acid and propofol glucuronidation with K_i values of 3.31 and 2.83 mM, respectively, in human liver microsomes. This suggests the possibility of pharmacokinetic interactions between ginsenoside Rc and drugs mainly metabolized by UGT1A9. The change in active drug exposure can also change drug efficacy. In spite of possible interactions in *in vitro* model, there has been no data yet in animals or humans investigating a drug interaction between ginsenoside Rc and mycophenolic acid, UGT1A9 probe substrate.[16]

Mycophenolic acid (Figure 1b) was developed as an immunosuppressant to complement existing immunosuppressive agents, including calcineurin inhibitor, azathioprine, and corticosteroids.[17] It has been used effectively after organ transplantation.[18] UGT1A9 is the major enzyme involved in the metabolism of mycophenolic acid to its glucuronide conjugate.[19] Drug interaction between mycophenolic acid as a probe substrate of UGT1A9 and other medications was

#These authors are equally contributed.
*Reprint requests to Kwang-Hyeon Liu
https://ordic.org/0000-0002-3285-5594
E-mail: dstlkh@knu.ac.kr

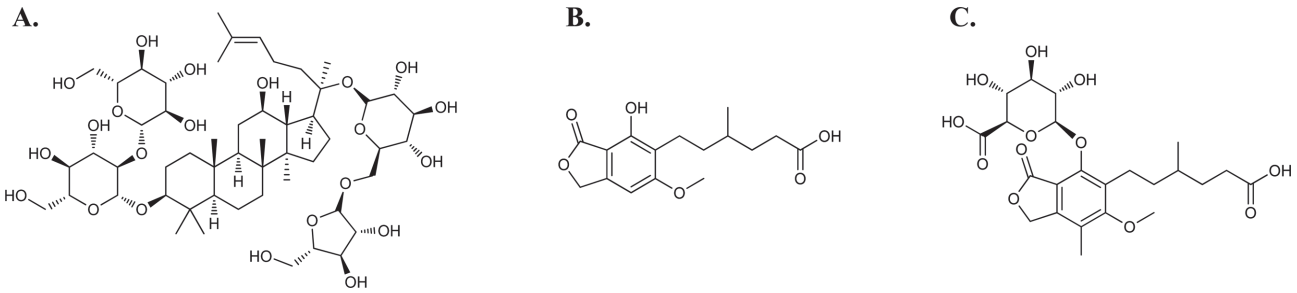

Figure 1. Chemical structures of ginsenoside Rc (A), mycophenolic acid (B), and mycophenolic acid-β-D-glucuronide (C).

performed. Rifampin induced systemic clearance of mycophenolic acid by inducing UGT1A9-mediated mycophenolic acid glucuronidation.[20] Failure to recognize this drug interaction might lead to mycophenolic acid underexposure and loss of clinical efficacy because mycophenolic acid has a narrow therapeutic window,[20] whereas increased plasma levels of toxic glucuronide metabolites could lead to side effects.

Although ginseng, particularly red ginseng, is one of the most commonly used herbal medicines in U.S.A. and Europe, no *in vivo* studies have been conducted to determine the effect of ginsenoside Rc, one of the most abundant ginsenosides, on UGT1A9 activity or interactions with other drugs. This study aimed to assess the effect of ginsenoside Rc on UGT1A9 activity in rats using mycophenolic acid glucuronidation as a UGT1A9 probe.

Experimental

Materials

Mycophenolic acid (MPA, purity > 98%) and estrone-β-D-glucuronide (EG) were purchased from Sigma-Aldrich (St. Louis, MO, U.S.A). Mycophenolic acid-β-D-glucuronide (MPAG, Figure 1c) was obtained from Toronto Research Chemicals (Toronto, ON, Canada). Ginsenoside Rc (GRc, purity > 98%) was obtained from Ambo Institute (Daejeon, Korea). Solvents were LC-MS grade (Fisher Scientific Co., Pittsburgh, PA, U.S.A).

Animal study

Male Sprague–Dawley rats (6–7 weeks old, 220–250 g) were purchased from Samtako Co. (Osan, Korea). The animals were acclimatized for one week in an animal facility at Kyungpook National University (Daegu, Korea). Food and water were provided ad libitum. The study protocol was approved by the Animal Care and Use Committee of Kyungpook National University (Approval No. KNU 2019-83). To calculate and compare the pharmacokinetic parameters of MPA and GRc, we conducted repeated blood sampling through the retro-orbital puncture under isoflurane anesthesia.[21]

Rats were randomized into three groups: a control group, single dose group, and multiple dose group, each consisting of four animals. The single dose group was intravenously injected once with GRc solution (5 mg/mL/kg, dissolved in saline) via the tail vein, while the multiple dose group was intravenously injected with GRc solution (3 mg/mL/kg, dissolved in saline) via the tail vein for five consecutive days. The control group received saline (1 mL/kg) via the tail vein. After 1 h following the last GRc treatment, MPA was intravenously injected into all groups via the tail vein at 2 mg/kg (dissolved in DMSO-saline = 2:8, *v*/*v*). Heparinized blood samples were taken at 0.17, 0.33, 0.67, 1.5, 2, 4, 8, 24, and 48 h following mycophenolic acid dosing via the retro-orbital vein. After centrifugation (16,000 g, 10 min, 4°C), aliquots (50 μL each) of plasma samples were stored at -80°C until the analysis of MPA and MPAG.

LC-MS/MS analysis of mycophenolic acid and its glucuronide

The concentration of MPA and MPAG was analyzed using a liquid chromatography coupled to a triple quadrupole mass spectrometry (LC-MS/MS) as previously reported by Wiesen et al.[22] with some modification. Briefly, acetonitrile (100 μL) including EG (IS) was added to the plasma samples (50 μL). After vortexing, the samples were centrifuged (16,000 g, 10 min, 4°C). A 5 μL sample of the supernatants was injected onto the LC-MS/MS.

MPA, MPAG, and the internal standard were quantified in a single run using a Shimadzu LCMS 8060 triple-quadrupole mass spectrometer coupled with a Nexera X2 ultra high performance liquid chromatography system (Shimadzu, Kyoto, Japan) equipped with an electrospray ionization interface. MPA, MPAG, and IS were separated on a Kinetex XB-C18 column (100 × 2.1 mm, 2.6 μm, Phenomenex, Torrance, CA, U.S.A). The mobile phase consisted of 0.1% formic acid in water (A) and 0.1% formic acid in acetonitrile (B), and was set as 0%→30% B (0–1 min), 30%→50% B (1–5 min), 50%→0% B (5–5.1 min), and 0% B (5.1–8 min). The flow rate was 0.2 mL/min. Electrospray ionization was performed in positive ionization mode at 4000 V or negative ionization mode at -3500 V. The optimum operating conditions were determined as follows: vaporizer temperature, 300°C; capillary temperature, 350°C; collision gas (argon) pressure, 1.5 m Torr. Quantification was conducted in the selected reaction

Table 1. Selected reaction monitoring (SRM) condition for mycophenolic acid, mycophenolic acid-β-D-glucuronide, and internal standard (IS)

Compound	SRM Transition (*m/z*)	Polarity	Collision Energe (eV)
Mycophenolic acid	321.2 > 207.0	+	-19
Mycophenolic acid-β-D-glucuronide	495.0 > 319.0	-	25
Estrone-β-D-glucuronide	455.0 > 269.0	-	35

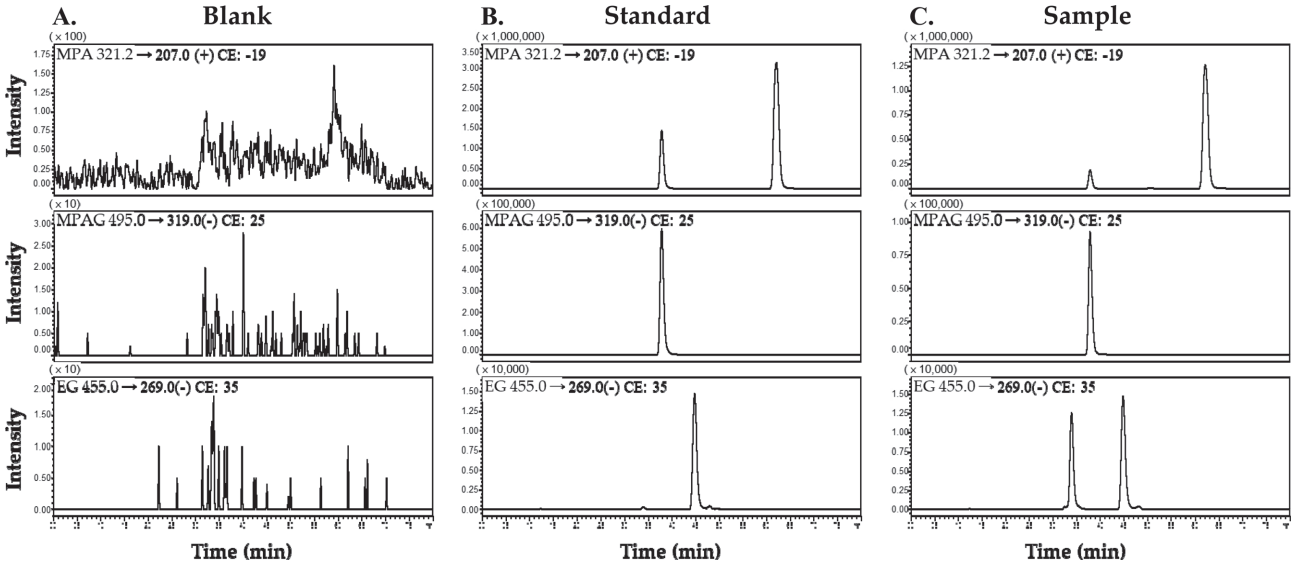

Figure 2. LC-MS/MS selected ion chromatograms of mycophenolic acid (MPA), mycophenolic acid-β-D-glucuronide (MPAG), and estrone-β-D-glucuronide (EG). Left column: blank plasma (A); middle column: plasma spiked with 5000 ng/mL of MPA and MPAG (B); right column: plasma sample equivalent to 2282.55, and 1676.78 ng/mL for MPA and MPAG, respectively, from rats 0.17 h after the intravenously injected dose of 3 mg/kg GRc and 2 mg/kg MPA.

monitoring (SRM) modes at *m/z* 321→207 for MPA (Collision energy, 19 eV), *m/z* 495→319 for MPAG (Collision energy, -25 eV), and *m/z* 455→269 for EG (Collision energy, -35 eV) (Table 1 and Figure 2). Analytical data were processed using a Shimadzu LabSolution LCMS software. Plasma calibration standards for the quantification of MPA and MPAG ranged from 20 to 5000 ng/mL, correlation coefficient (r^2) ranged from 0.995 to 0.998, and the intraday and interday accuracy ranged from 86.8% to 109.7%. The intraday and interday precision ranged from 1.0% to 7.8%.

Data analysis

The pharmacokinetic parameters of MPA and MPAG were calculated from plasma concentration-time profiles using a non-compartment analysis of WinNonlin software (version 5.1; Pharsight, Cary, NC, U.S.A). GraphPad Prism (version 6.0; GraphPad, San Diego, CA, U.S.A) was used for statistical analysis. The estimated parameters obtained from the control and single or multiple dose groups were statistically compared using Student's t-test. Statistical significance was assessed at a level of $p < 0.05$.

Results and Discussion

So far, only one drug interaction study between mycophenolic acid, a UGT1A9 probe drug, and other drugs has been conducted. Rifampin co-administration with mycophenolic acid increased area under the plasma concentration-time curve (AUC) value of mycophenolic acid by induction of UGT1A9 glucuronidation activity.[20] However, there have been no studies on drug interactions based on the inhibition of UGT1A9 enzyme activity. In this study, therefore, we investigated the UGT1A9 inhibitory effects of ginsenoside Rc, a strong and selective UGT1A9 inhibitor, on the pharmacokinetics of mycophenolic acid, a UGT1A9 probe drug. GRc was intravenously injected to maximize the plasma concentration, thus, the UGT1A9 inhibitory potential of GRc.

Co-administration of MPA and GRc resulted in the lack of herb-drug interaction (HDI) between GRc and MPA. Mean plasma concentration-time profiles of MPA and MPAG in the absence or presence of either single dose GRc (5 mg/mL/kg, iv) or repeated dose GRC (3 mg/mL/kg/day, iv for five days) in rats were similar (Figure 3), and relevant pharmacokinetic parameters of MPA and MPAG

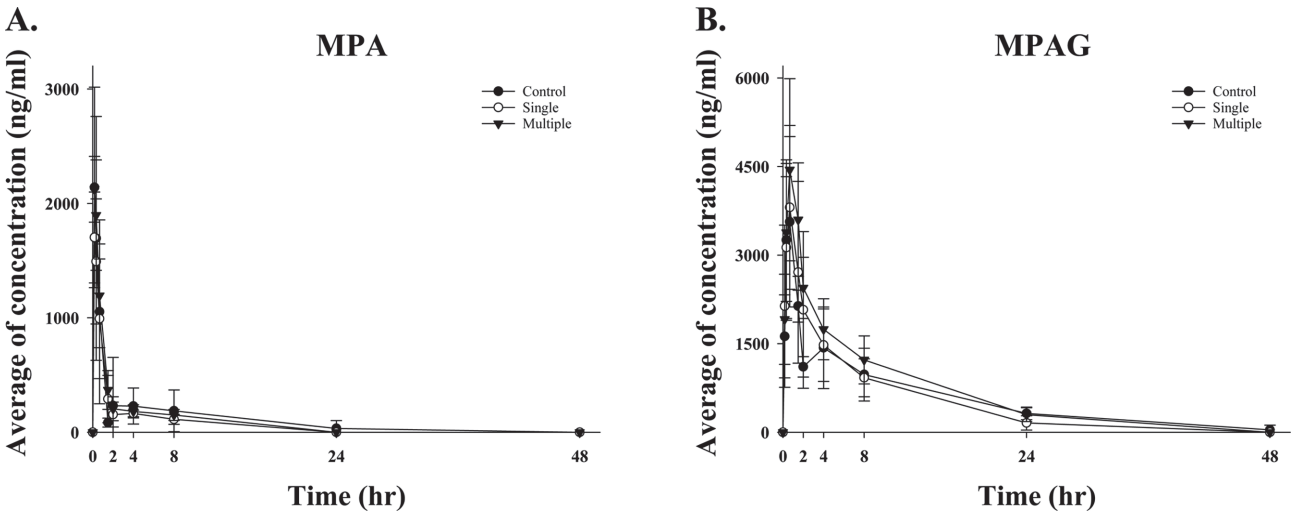

Figure 3. (A) Plasma concentration-time profile of mycophenolic acid (MPA) in the control, single dose (ginsenoside Rc 5 mg/mL/kg), and multiple dose (ginsenoside Rc 3 mg/mL/kg for 5 days) groups following intravenous injection of MPA at a dose of 2 mg/kg in rats (mean ± SD, n = 4). (B) Plasma concentration-time profile of mycophenolic acid-β-D-glucuronide (MPAG) in the control, single dose (ginsenoside Rc 5 mg/mL/kg), and multiple dose (ginsenoside Rc 3 mg/mL/kg for 5 days) groups following intravenous injection of MPA at a dose of 2 mg/kg in rats (mean ± SD, n = 4).

Table 2. Pharmacokinetic parameters of mycophenolic acid in control, single dose (ginsenoside Rc 5 mg/mL/kg), and multiple dose (ginsenoside Rc 3 mg/mL/kg for five days) groups following intravenous injection of MPA at a dose of 2 mg/kg in rats (mean ± SD, n = 4).

Mycophenolic acid			
Parameters	Control	Single Dose	Multiple Dose
$T_{1/2}$ (h)	5.24 ± 4.71	6.20 ± 5.89	3.75 ± 2.82
C_0 (ng/mL)	2141.97 ± 874.61	1766.55 ± 326.61	2135.04 ± 293.88
AUC_{48h} (ng·h/mL)	3975.91 ± 4561.37	2344.61 ± 825.57	2878.11 ± 859.44
AUC_{∞} (ng·h/mL)	5611.19 ± 6338.15	3459.07 ± 1741.85	3618.36 ± 971.81
MRT (h)	3.39 ± 2.18	2.17 ± 0.09	2.16 ± 0.22
CL (mL/h/kg)	0.85 ± 0.47	0.82 ± 0.63	0.62 ± 0.20
Vd (L/kg)	1.04 ± 0.35	1.16 ± 0.20	0.95 ± 0.15

Data represent mean ± SD of four rats per group. $T_{1/2}$: elimination half-life; C_0: initial plasma concentration at 1 h; AUC_{48h} or AUC_{∞}: Area under the plasma concentration-time curve from zero to 24 h or infinity; *MRT*: mean residence time; *CL*: systemic clearance; *Vd*: Volume of distribution.

Table 3. Pharmacokinetic parameters of mycophenolic acid-β-D-glucuronide (MPAG) in control, single dose (ginsenoside Rc 5 mg/mL/kg), and multiple dose (ginsenoside Rc 3 mg/mL/kg for five days) groups following intravenous injection of MPA at a dose of 2 mg/kg in rats (mean ± SD, n = 4).

Mycophenolic acid-β-D-glucuronide			
Parameters	Control	Single Dose	Multiple Dose
$T_{1/2}$ (h)	14.33 ± 10.41	7.04 ± 2.80	7.96 ± 1.31
T_{max} (h)	0.58 ± 0.17	0.50 ± 0.19	0.88 ± 0.42
C_{max} (ng/mL)	3630.31 ± 1475.59	3953.17 ± 1362.24	4574.31 ± 1318.95
AUC_{48h} (ng·h/mL)	23253.83 ± 6861.06	20244.47 ± 7567.91	29087.93 ± 8185.30
AUC_{∞} (ng·h/mL)	28691.08 ± 6209.48	23724.83 ± 7667.03	32610.42 ± 9009.45
MRT (h)	9.58 ± 4.73	5.57 ± 1.82	6.45 ± 0.61

Data represent mean ± SD of four rats per group. $T_{1/2}$: elimination half-life; T_{max}: time to reach C_{max}; C_{max}: maximum plasma concentration; AUC_{48h} or AUC_{∞}: Area under the plasma concentration-time curve from zero to 24 h or infinity; *MRT*: mean residence time.

are listed in Table 2 and Table 3. In the MPA alone group, the mean C_0 and AUC_{inf} were 2.14 mg/mL and 5.61 mg×h/mL, respectively, and *CL* is 0.85 mL/h/kg. Single dose GRc did not affect the pharmacokinetics of MPA (Table 4). To achieve the highest and stable plasma concentration of GRc, GRc was intravenously injected for five days before MPA administration. However, the plasma concentration of MPA was not affected by repeated GRc treatment (Figure 2), and all pharmacokinetic parameters were not statistically different between the two groups (Table 2). We also calculated pharmacokinetic parameters of MPAG, UGT1A9 specific metabolite of MPA (Table 3). Similar to MPA, there was no significant difference in pharmacokinetic parameters of MPAG among three groups (control, single dose GRc, and multiple dose GRc) (Table 3).

Jeon et al. reported that GRc showed high protein binding in rat plasma and liver homogenates (> 99.5%) and was not widely distributed to the liver with a liver-to-plasma concentration ratio of 0.13-0.2.[23] High protein binding and limited liver distribution of GRc might contribute to the lack of pharmacokinetic HDI involving MPA in rats although their plasma concentration was maximized following intravenous injection of GRc. Jiang et al. also reported that the unbound fraction of GRc was low (0.6%) in human plasma.[24] Based on the similarity in the protein binding features between rats and humans[23,24] and inhibitory effect on UGT1A9 of GRc, no HDI between MPA and GRc would be expected in humans.

UGT1A9 is one of the most essential UGT isoforms abundantly expressed in human's liver and kidney.[25] Human UGT1A9 had been regarded as a minor hepatic drug-metabolizing enzyme, with 1.78% hepatic expression. However, it represents above 50% of the total kidney UGT content.[25] UGT1A9 was suggested to be responsible for the hepatic glucuronidation of 16% of 200 top prescribed drugs in the United States in 2002.[26,27] UGT1A9 is essential UGT isoform responsible for the metabolism of endogenous estrogen and various therapeutic drugs such as dapagliflozin, edaravone, entacapone, morinidazole, mycophenolic acid, propofol, and sulfinpyrazone.[28] Therefore, the findings showing the lack of HDI between GRc and mycophenolic acid would provide helpful information for patients taking drugs that are mainly metabolized by UGT1A9 such as mycophenolic acid and propofol.

Conclusions

In conclusion, the present findings suggest that ginsenoside Rc has no statistically significant effects on the pharmacokinetics of mycophenolic acid and its glucuronide metabolites in rats. Additionally, considering high protein binding and limited liver distribution of GRc, no HDI between UGT1A9 substrate drug and GRc would also be expected in humans.

Acknowledgements

This research was supported by the National Research Foundation of Korea, Ministry of Science and ICT, Republic of Korea [Grant NRF-2019R1A2C1008713], and by a Korea Basic Science Institute National Research Facilities & Equipment Center grant funded by the Korea government (Ministry of Education) [Grant 2019R1A6C1010001].

References

1. Ru, W.; Wang, D.; Xu, Y.; He, X.; Sun, Y. E.; Qian, L.; Zhou, X.; Qin, Y. *Drug Discov. Ther.* **2015**, 9, 23, DOI: 10.5582/ddt.2015.01004.
2. Heo, S. B.; Lim, S. W.; Jhun, J. Y.; Cho, M. L.; Chung, B. H.; Yang, C. W. *J. Ginseng Res.* **2016**, 40, 18. DOI: 10.1016/j.jgr.2015.04.005.
3. Lee, M. J.; Jang, M.; Choi, J.; Chang, B. S.; Kim, D. Y.; Kim, S. H.; Kwak, Y. S.; Oh, S.; Lee, J. H.; Chang, B. J.; Nah, S. Y.; Cho, I. H. *Mol. Neurobiol.* **2016**, 53, 1977, DOI: 10.1007/s12035-015-9131-4.
4. Attele, A. S.; Wu, J. A.; Yuan, C. S. *Biochem. Pharmacol.* **1999**, 58, 1685, DOI: 10.1016/s0006-2952(99)00212-9.
5. Fang, Z. Z.; Cao, Y. F.; Hu, C. M.; Hong, M.; Sun, X. Y.; Ge, G. B.; Liu, Y.; Zhang, Y. Y.; Yang, L.; Sun, H. Z. *Toxicol. Appl. Pharmacol.* **2013**, 267, 149, DOI: 10.1016/j.taap.2012.12.019.
6. Sun, L.; Ropartz, D.; Cui, L.; Shi, H.; Ralet, M. C.; Zhou, Y. *Carbohydr. Polym.* **2019**, 203, 119, DOI: 10.1016/j.carbpol.2018.09.045.
7. Baeg, I. H.; So, S. H. *J. Ginseng Res.* **2013**, 37, 1, DOI: 10.5142/jgr.2013.37.1.
8. Qi, L. W.; Wang, C. Z.; Yuan, C. S. *Phytochemistry* **2011**, 72, 689, DOI: 10.1016/j.phytochem.2011.02.012.
9. Xie, J. T.; McHendale, S.; Yuan, C. S. *Am. J. Chin. Med.* **2005**, 33, 397, DOI: 10.1142/S0192415X05003004.
10. Cho, W. C.; Chung, W. S.; Lee, S. K.; Leung, A. W.; Cheng, C. H.; Yue, K. K. *Eur. J. Pharmacol.* **2006**, 550, 173, DOI: 10.1016/j.ejphar.2006.08.056.
11. Paul, S.; Shin, H. S.; Kang, S. C. *Food Chem. Toxicol.* **2012**, 50, 1354, DOI: 10.1016/j.fct.2012.02.035.
12. Abdulridha, M. K.; Al-Marzoqi, A. H.; Al-Awsi, G. R. L.; Mubarak, S. M. H.; Heidarifard, M.; Ghasemian, A. *J. Gastrointest. Cancer* **2020**, 51, 765, DOI: 10.1007/s12029-020-00385-0.
13. Lee, M. S.; Hwang, J. T.; Kim, S. H.; Yoon, S.; Kim, M. S.; Yang, H. J.; Kwon, D. Y. *J. Ethnopharmacol.* **2010**, 127, 771, DOI: 10.1016/j.jep.2009.11.022.
14. Chu, Y.; Zhang, H. C.; Li, S. M.; Wang, J. M.; Wang, X. Y.; Li, W.; Zhang, L. L.; Ma, X. H.; Zhou, S. P.; Zhu, Y. H.; Liu, C. X. *J. Chromatogr. B* **2013**, 919-920, 75, DOI: 10.1016/j.jchromb.2012.12.022.
15. Lee, S. M.; Bae, B. S.; Park, H. W.; Ahn, N. G.; Cho, B. G.; Cho, Y. L.; Kwak, Y. S. *J. Ginseng Res.* **2015**, 39, 384.
16. Lee, H.; Heo, J. K.; Lee, G. H.; Park, S. Y.; Jang, S. N.; Kim, H. J.; Kwon, M. J.; Song, I. S.; Liu, K. H. *Drug Metab.*

Dispos. **2019**, 47, 1372, DOI: 10.1124/dmd.119.087965.
17. Allison, A. C.; Eugui, E. M. *Transplantation* **2005**, 80, S181, DOI: 10.1097/01.tp.0000186390.10150.66.
18. Staatz, C. E.; Tett, S. E. *Arch. Toxicol.* **2014**, 88, 1351, DOI: 10.1007/s00204-014-1247-1.
19. Picard, N.; Ratanasavanh, D.; Premaud, A.; Le Meur, Y.; Marquet, P. *Drug Metab. Dispos.* **2005**, 33, 139, DOI: 10.1124/dmd.104.001651.
20. Naesens, M.; Kuypers, D. R.; Streit, F.; Armstrong, V. W.; Oellerich, M.; Verbeke, K.; Vanrenterghem, Y. *Clin. Pharmacol. Ther.* **2006**, 80, 509, DOI: 10.1016/j.clpt.2006.08.002.
21. Li, L.; Yu, P.; Zhang, P.; Wu, H.; Chen, Q.; Li, S.; Wang, Y. *Cancer Med.* **2020**, 9, 2491, DOI: 10.1002/cam4.2866.
22. Wiesen, M. H. J.; Farowski, F.; Feldkötter, M.; Hoppe, B.; Müller, C. *J. Chromatogr. A* **2012**, 1241, 52, DOI: 10.1016/j.chroma.2012.04.008.
23. Jeon, J. H.; Lee, S.; Lee, W.; Jin, S.; Kwon, M.; Shin, C. H.; Choi, M. K.; Song, I. S. *Molecules* **2020**, 25, 622, DOI: 10.3390/molecules25030622.
24. Jiang, R.; Dong, J.; Li, X.; Du, F.; Jia, W.; Xu, F.; Wang, F.; Yang, J.; Niu, W.; Li, C. *Br. J. Pharmacol.* **2015**, 172, 1059, DOI: 10.1111/bph.12971.
25. Ohno, S.; Nakajin, S. *Drug Metab. Dispos.* **2009**, 37, 32, DOI: 10.1124/dmd.108.023598.
26. Williams, J. A.; Hyland, R.; Jones, B. C.; Smith, D. A.; Hurst, S.; Goosen, T. C.; Peterkin, V.; Koup, J. R.; Ball, S. E. *Drug Metab. Dispos.* **2004**, 32, 1201, DOI: 10.1124/dmd.104.000794.
27. Burchell, B.; Lockley, D. J.; Staines, A.; Uesawa, Y.; Coughtrie, M. W. *Methods Enzymol.* **2005**, 400, 46, DOI: 10.1016/S0076-6879(05)00003-0Get.
28. Lv, X.; Zhang, J. B.; Hou, J.; Dou, T. Y.; Ge, G. B.; Hu, W. Z.; Yang, L. *Biotechnol. J.* **2019**, 14, e1800002, DOI: 10.1002/biot.201800002.

Author Guidelines

Aims and Scope

Mass Spectrometry Letters publishes brief letters (maximum length of 4 pages), technical notes, articles, reviews, and tutorials on fundamental research and applications in all areas of mass spectrometry. The manuscripts can be either invited by the editors or submitted directly by authors to the journal editors. Mass Spectrometry Letters topical sections are diverse, covering ion chemistry in a broad sense; gas-phase thermodynamics or kinetics; theory and calculations related with mass spectrometry or ions in vacuum; ion-optics; analytical aspects of mass spectrometry; instrumentations; methodology developments; ionization methods; proteomics and its related research; metabolomics and its related research; bioinformatics; software developments; database development; biological research using mass spectrometry; pharmaceutical research by mass spectrometry; food sciences using mass spectrometry; forensic results using mass spectrometry; environmental mass spectrometry; inorganic mass spectrometry; chromatography-mass spectrometry; tandem mass spectrometry; small molecule research using mass spectrometry; TOF-SIMS, etc. The scope of Mass Spectrometry Letters is not limited to the above-mentioned areas, but includes ever-expanding areas related directly or indirectly to mass spectrometry. Criteria for publication are originality, urgency, and reportable values. Short preliminary or proof-of-concept results, which will be further detailed by the following submission to other journals, are recommended for submission.

The publication frequency

Mass Spectrometry Letters will be published at least four times a year; 31th March, 30th June, 30th September, 31th December every year are the scheduled publishing dates. The publication frequency is subjected to future change, which should be advised by the Editorial board meeting's decisions.

The publication charge

All the papers will be published for free without any payment of page charge or article processing charge and the access to the papers in Mass Spectrometry Letters is also free to the public in general through the homepage of the journal. The publication cost will be covered by the Korean Society for Mass Spectrometry. The printed journal issue will be provided to the Korean Society for Mass Spectrometry members who have completed the annual membership fee payment.

The copyright

All MS Letters content is Open Access, meaning it is accessible online to everyone, without fee and authors' permission. All MS Letters content is published and distributed under the terms of the Creative Commons Attribution License (Http://creativecommons.org/licenses/by/3.0/). Under this license, authors reserve the copyright for their content; however, they permit anyone to unrestrictedly use, distribute, and reproduce the content in any medium as far as the original authors and source are cited. For any reuse, redistribution, or reproduction of a work, users must clarify the license terms under which the work was produced.

Referee Reviews

Submitted manuscripts are subjected to review by at least 2 referees selected by the editors. The authors can recommend preferred potential reviewers with the names and e-mail addresses. Note that the editor retains the sole right to decide whether or not the suggested reviewers are used.

Conflict of interest

All authors are requested to disclose any actual or potential conflict of interest including any financial, personal or other relationships with other people or organizations within three years of beginning the submitted work that could inappropriately influence, or be perceived to influence, their work.

Submission declaration and verification

Submission of an article implies that the work described has not been published previously (except in the form of an abstract or as part of a published lecture or academic thesis), that it is not under consideration for publication elsewhere, that its publication is approved by all authors and tacitly or explicitly by the responsible

authorities where the work was carried out, and that, if accepted, it will not be published elsewhere in the same form, in English or in any other language, including electronically without the written consent of the copyright-holder. To verify originality, your article may be checked by the originality detection software.

Research/publication ethics and research/publication malpractice statement

For the policies on the research and publication ethics not stated in these instructions, international standards for editors and authors (http://publicationethics.org/international-standards-editors-and-authors) can be applied.

Language and language services

The manuscript should be prepared in good English (American or British usage is accepted, but not a mixture of these). English language proof-reading service is recommended before publication.

Submission

Submission to this journal proceeds totally online and you will be guided stepwise through the creation and uploading of your files.

Manuscript Types

Mass Spectrometry Letters publishes several types of articles: letter, technical note, article, review, and tutorial.

· **Review.** A comprehensive overview on a topic in mass spectrometry. There is no restriction in length.

· **Article.** A full-length article presenting important new research results. The length of the articles should not exceed ten printed pages.

· **Technical note.** A short description of a novel apparatus of technique. The length of technical notes should not exceed three printed pages.

· **Letter.** A short report on any subject in mass spectrometry, requiring urgency, timeliness, and scientific significance. The length of letters should not exceed four printed pages.

· **Tutorial.** A tutorial is an educational exposition covering recent trends and basic knowledge in mass spectrometry. There is no restriction in length

All manuscripts for publication in Mass Spectrometry Letters, except review and tutorial, should include Title, Authors, Abstract, Introduction, Experimental section, Results and Discussion, Conclusions, Acknowledgments, and References.

Preparation of Manuscripts

All the manuscripts for publication in Mass Spectrometry Letters should be prepared in English. Authors are strongly recommended to use the manuscript template (Manuscript Template) provided from the Mass Spectrometry Letters website.

1) Manuscript type

The type of a manuscript should be specified in the cover letter.

2) Title

The title should be concise and informative. Authors are strongly recommended to limit the title to 250 letters including space, and to avoida bbreviations and formulae wherever possible. A short running title consisting of less than 70 letters including space should be provided by authors.

3) Authors

List full names of all authors (given names first and surnames last) followed by the authors' affiliations and addresses where the actual work was carried out. Superscript numbers are labeled after the authors' names and in front of the appropriate affiliations. Specify current addresses, if necessary, as footnotes. Provide the full postal address of each affiliation including the country name. Corresponding author(s) should beindicated with asterisk symbols. The email address(es) of corresponding author(s) are additionally required in the manuscript.

4) Abstract

The abstract should not exceed 250 words. It should be a single paragraph which summarizes the content of the article.

5) Introduction

The introduction should state the purpose and the backgrounds of thework. It may include appropriate citations of previous works with brief summaries. Do not include or summarize current findings in this section.

6) Experimental section

Authors should provide details on experimental procedures including the model names, the manufactures of instruments, and reagents, so that the works are reproducible elsewhere by readers.

7) Results and discussion

Authors should provide the results of the work with clear and concise manners. Authors should discuss the significance of observations, measurements, or computations.

8) Conclusion

A brief summary should be provided in conclusions.

9) Acknowledgements

Provide a list of financial supports and individuals whom to be acknowledged.

10) References

Literatures to be cited should be numbered by order of appearance in the manuscript. The corresponding texts should be indicated with superscripted Arabic numbers (e.g., 1). The reference format must follow the examples provided below. Unpublished results are not allowed in the reference list with an exception of the literatures accepted for publication as "in press".

<Journals>

Hong, E. S.; Yoon, H.-J.; Kim, B.; Yim, Y.-H.; So, H.-Y.; Shin, S. K. *J. Am. Soc. Mass Spectrom.* **2010**, 21, 1245, DOI: 10.1016/j.jasms.2010.03.035

<Books>

Bunker, P. R.; Jensen, P. Molecular Symmetry and Spectroscopy, 2nd ed.. NRC Research Press: Ottawa, 1998.

Zare, R. N. Angular Momentum, Wiley: New York, 1998.

<Software>

Werner, H. J.; Knowles, P. J.; Lindh, R.; Manby, F. R.; Schutz, M. MOLPRO, version 2006. 1., A package of ab initio Programs; See http://www.molpro.net.

<Proceedings>

Bensaude-Vincent, B. The New Identity of Chemistry as Biomimetic and Nanoscience; 6th International Conferenceon the History of Chemistry, Leuven (Belgium), August 28 - September 1, 2007, p 53.

11) Equations and math formulae

Equations and math formulae should be prepared by Microsoft Equation 3.0 (or a later version). All the equations and math formulae should be numbered by order of appearance in the manuscript with Arabic numbers.

12) Tables

Tables should be numbered by order of appearance in the manuscript with Arabic numbers. Each table should have a brief title. Footnotes may be placed, if necessary, to supplement the tables. Avoid vertical rules. The size of table should fit the MSL's page (16.5 cm × 22.5 cm).

13) Figures

Figures should be numbered by order of appearance in the manuscript with Arabic numbers. Each figure should have a brief title followed by a brief description, which consists of one or two sentences. Sub-numbering is possible with lowercase alphabets (e.g., a, b, etc.), if necessary. The resolution of a figure should be better than 600 dpi. JPEG (jpg, Joint Photographic Expert Group) format is recommended.

14) Units

SI units rather than conventional units should be used for reporting measures. Information regarding on SI units can be found at https://www.nist.gov/pml/weights-and-measures/metric-si/si-units.

Academic Data Analysis Software Program

Get 25 free data analysis software licenses with the purchase of Agilent instrument software

The Agilent Academic Data Analysis Software Program supports teachers, students and researchers with free copies of Agilent data analysis software for educational use.

The installation of data analysis software on multiple computers can transform a lab course from passive to active and from theoretical to applied.

Software products eligible for the program are:

- Chromatography systems
  - OpenLab CDS Workstation
  - OpenLab CDS ChemStation Edition*
- HPLC, GC & ICP mass spectrometry systems
  - MassHunter Workstation
  - MassHunter PCDL*
- ICP-OES, MP-AES, Cary60/100/300/4000/5000/6000i/7000 UMS/8454 UVVIS/Eclipse/630 FTIR
  - SpectrAA
  - ICP Expert 7
  - MP Expert
  - UV-Visible ChemStation
  - Cary Win FLR*
  - MircoLab

**OpenLab CDS ChemStation Edition, MassHunter PCDL, and Cary Win FLR are only eligible for 5 free additional licenses of data analysis software.*

Building Better Science

Agilent supports and enables Academics to achieve their goals through a variety of programs.

Learn more at:
https://www.agilent.com/en/academia

Contact your Agilent representative to discuss your needs.

For Research Use Only. Not for use in diagnostic procedures.

This information is subject to change without notice.

Published in the USA, August 15, 2018
5994-0161EN

Agilent
Trusted Answers

thermo scientific

Leading performance

The performance to drive discovery and identification, plus the quantitative precision and accuracy you need to confidently scale up and achieve impact—with operational simplicity and fast time-to-results.

Meet the Thermo Scientific™ Orbitrap Exploris™ 240 mass spectrometer: leading performance, application versatility and intelligent data acquisition enable exceptional data quality that is synonymous with Thermo Scientific™ Orbitrap™ technology. Discover your fast track to confident results.

Performance | Versatility | Operational Simplicity

Find out more at **thermofisher.com/OrbitrapExploris240**

ThermoFisher SCIENTIFIC

www.waters.com/kr

Waters
THE SCIENCE OF WHAT'S POSSIBLE.™

IMS beyond your imagination

SELECT SERIES Cyclic IMS

SELECT SERIES Cyclic IMS는 고도의 협력을 통해 개발된 제품으로 신기술인 Cyclic Ion Mobility 분리 기술과첨단 고성능 ToF(time-of-flight) 질량분석기를 결합하여 연구자가 과학적인 발견 단계에서 잠재력을 발휘할 수 있도록 지원합니다.

SELECT SERIES Cyclic IMS

Waters Corporation
서울특별시 영등포구 여의공원로 101 CCMM 빌딩 905~7호, 07241
전화: 02 6300 9200 팩스: 02 6300 9205 www.waters.com/kr

PHARMACEUTICAL ▪ HEALTH SCIENCES ▪ FOOD ▪ ENVIRONMENTAL ▪ CHEMICAL MATERIALS

timsTOF fleX MALDI 2

MALDI Guided SpatialOMx

timsTOF fleX uniquely enables SpatialOMx

PASEF powered LC-MS/MS identification matched with spatial localization identifies and locates multilevel genomic expression in tissue without labels

timsTOF fleX provides results without compromise

All the 4D-Omics power that you demand from proven PASEF workflows with fast, software-controlled changeover to MALDI for rapid molecular imaging

timsTOF fleX allows you to work smarter

Label-free mapping of metabolites, lipids, glycans, peptides and more can efficiently direct your deep 4D-Omics studies with laser guided precision so that you focus on the tissue regions that matter.

For research use only. Not for use in clinical diagnostic procedures.

Bruker Daltonik GmbH

경기도 성남시 분당구 판교로 338 KTNET 4층 브루커코리아
Tel. 031-712-9933 Fax. 031-712-9933
E-mail: Info.BDAL.KR@bruker.com

Scan the QR-Code for more Details

YOUNG IN Chromass
www.youngcm.com
mkt@youngincm.com

YOUNG IN ACE
www.younginace.com
sales@younginace.com

YOUNG IN
High-End Mass Spectrometry Portfolio

ACE 1000 IMR-MS
Ion Molecule Reaction Mass Spectrometer

- FAST analysis – direct analysis can save analysis time
- REAL TIME analysis – based on fast analysis time, immediately getting a result with real time
- ACCURATE result – simple mass spectrum makes it easy to confirm result
- ON SITE analysis – can be used in the point of analysis is required

ChroZen TQ GC/MS

- Axial Ion Source
- 90° Curved Active Focusing q0
- 180 ° curved collision cell (Zero Cross-Talk)
- Fast scan rate : 30,000 amu/s
- Maximum MRM Acquisition : 1,000MRM/sec
- Target monitoring of trace level substances in air/water

- 180 ° curved collision cell (Zero Cross-Talk)
- Simultaneous multi-component analysis of various concentrations of compounds with excellent linearity
- Target monitoring of trace level substances in water

KSMS Korean Society for Mass Spectrometry